MULTICOLOR ANALYSIS OF STARS & GALAXIES

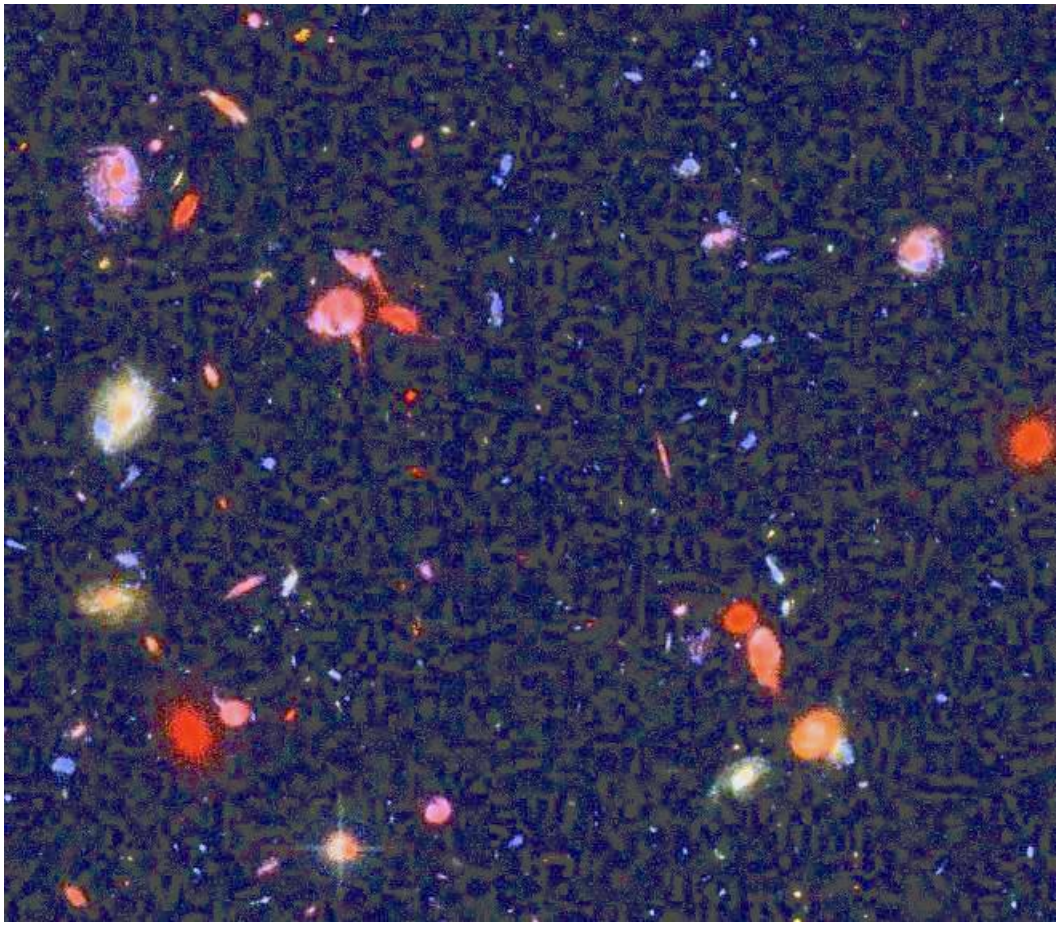

Hubble Ultra Deep Field (Luptonized)

MULTICOLOR ANALYSIS: INTRODUCTION

Probably the most influential application of multicolor analysis of stars has been in the form of color-magnitude diagrams (CMD's). Photoelectric photometry allows high precision CMD comparisons between theory and observation which in the last 50 years have provided a nearly complete understanding of stellar evolution from the main sequence through giant phases. But we can't discuss that vast(!) undertaking here. See ASTR 551 (Majewski) and ASTR 543 (Li) for examples. Instead, we focus here on what can be learned from color-color diagrams and other forms of multicolor analysis, which have many applications beyond stellar evolution.

I. THE UBV TWO-COLOR DIAGRAM: Stellar Temperatures, Gravities, Abundances

The Johnson & Morgan UBV system was defined (see filter specifications in Lec. 14) such that:

> **(U-B) measures the "Balmer Jump" (hot stars) or the "4000 Å break" (cooler stars) between 3600 Å and 4400 Å.**
>
> **(B-V) measures the slope of the "Paschen continuum" between 4400 Å and 5500 Å; sensitive to stellar temperature**
>
> **The U band is sensitive to stellar surface gravity (g) and metal abundance (Z) as well as temperature.**
>
> **The UBV system demonstrates that simple observations can be powerful astrophysical discriminants**

The standard "two-color diagram" plots (B-V) vs. (U-B)

> **Sense of plot is such that hottest objects (bluer) are in upper left of diagram, coolest in lower right (redder)**
>
> **Stars are confined to a relatively small domain of 2-color space. (Why?)**
>
> **Temperature is the dominant parameter, but g and Z are also important**
>
> **Most conspicuous feature: "dwarf" (Class V) line: a locus of varying temperature/spectral type.**

UBV TWO-COLOR DIAGRAM (continued)

The S-curve is introduced by the Balmer Jump (i.e. continuum absorption for $\lambda < 3650$ Å by neutral hydrogen in $n = 2$ level), which reaches a maximum near $T = 10000$ K (early A stars).

Surface gravity affects the ionization of absorbers in an atmosphere through gas pressure. For a given T, lower gravity implies lower gas pressure and therefore higher ionization. For instance, near $T = 10000$ K, there will be more neutral hydrogen in the atmosphere of a dwarf (high gravity) than a supergiant.

For FG stars, (U-B) is very sensitive to "line blanketing" by metals and therefore to Z. Lower Z stars have a "UV excess" (more short wavelength light for a given long wavelength spectral slope).

The ability of the UBV diagram to separate out stars by temperature and abundance has made it a major tool in study of stellar populations in our own & other galaxies.

The UBV diagram also allows identification of special types of sources (e.g. QSO's, brown dwarfs, white dwarfs) by colors alone.

Fiducial (U-B), (B-V) values:

Object	(U-B)	(B-V)
Hottest Stars	-1.1	-0.32
A0 V	0.0	0.0
Sun (G2 V)	0.17	0.68
M5	1.20	1.60
Carbon Star	8.0	5.0

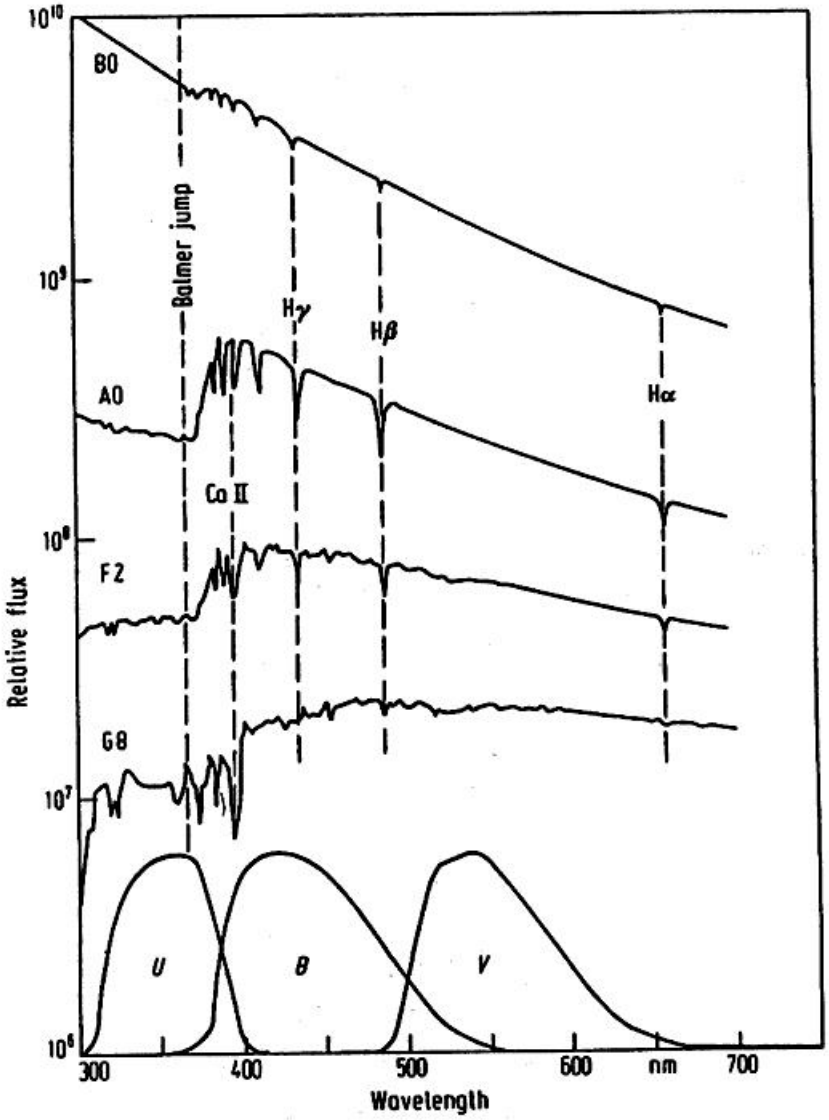

Location of the UBV Filters (Johnson & Morgan 1953)

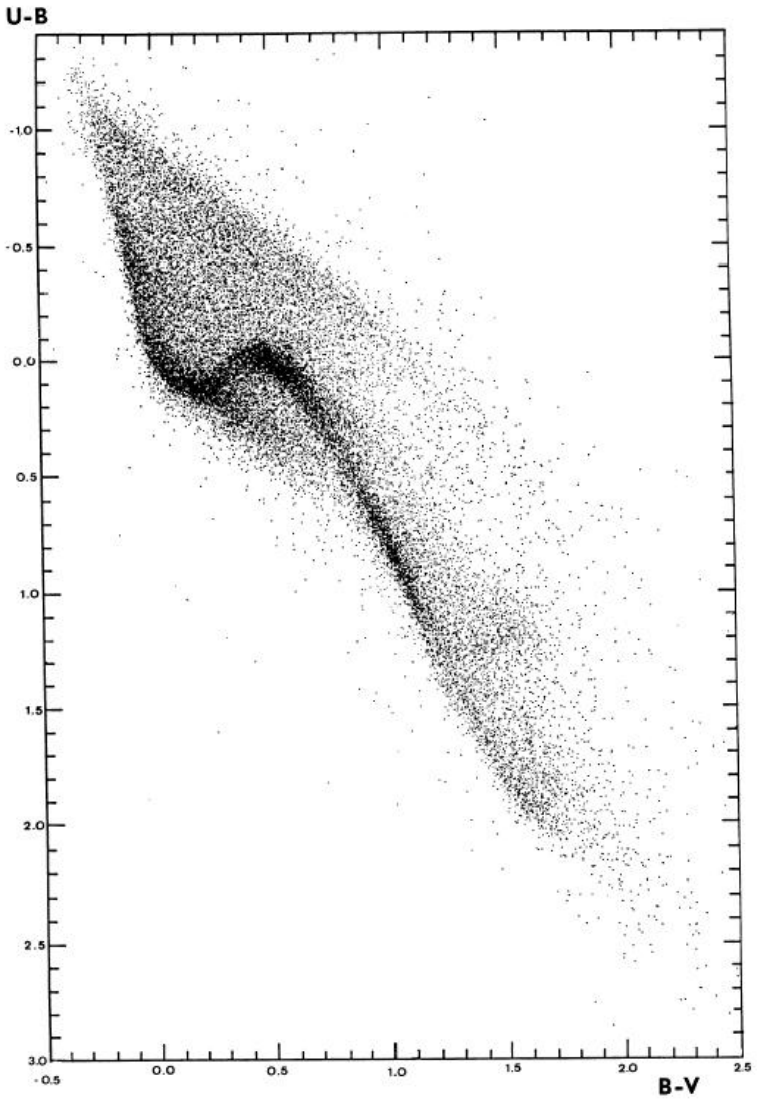

Composite 2-Color Diagram (Nicolet 1980)

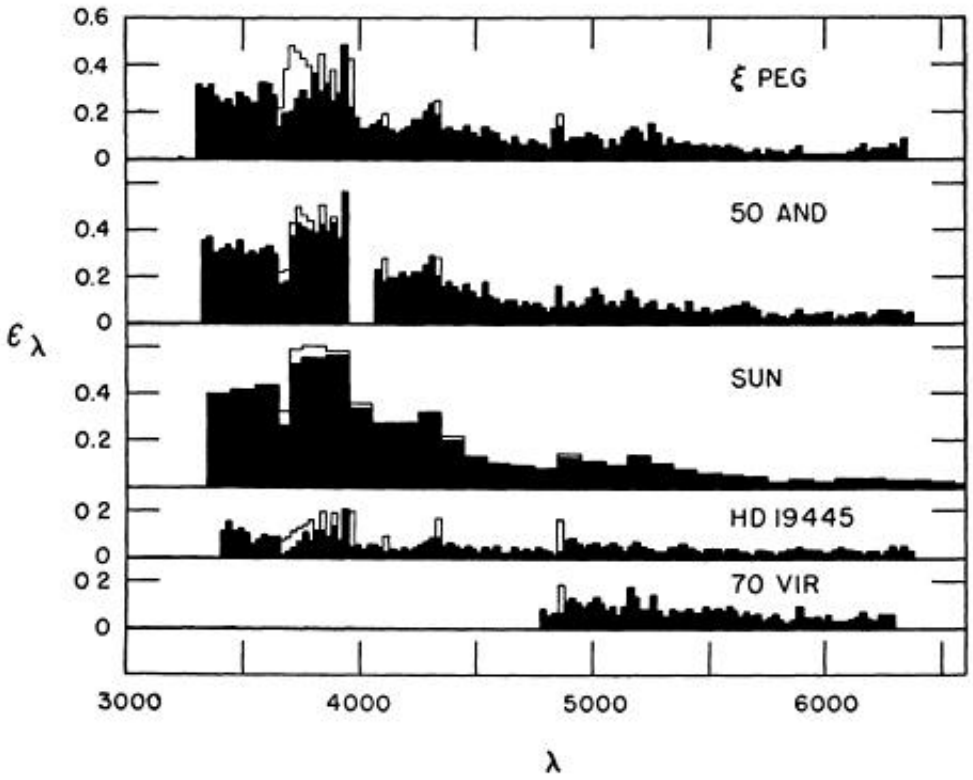

FIG. 1.—The fractional blocking coefficients, $\epsilon(\lambda)$, for the program stars. The data for the sun are from Michard (1950). The non-filled areas of the histograms represent absorption by the hydrogen lines.

Line Blanketing in Stars (Wildey et al. 1962)

The plot shows the amount of energy removed by absorption features as a function of wavelength.

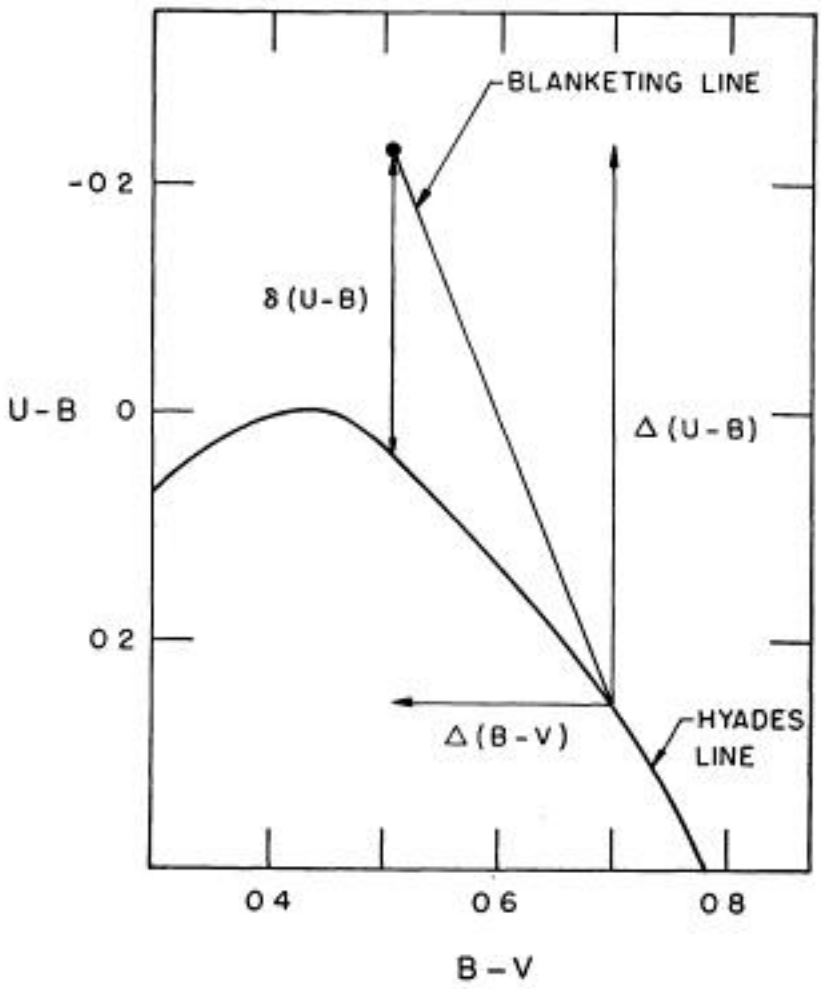

FIG. 5.—The definitions of $\Delta(B-V)$, $\Delta(U-B)$, and the ultraviolet excess, $\delta(U-B)$

Definition of the "UV Excess" for Cool Subdwarfs

The diagonal line shows how a star of a given T_e, g will move if its metal abundance is reduced from solar (on the "Hyades line") to Pop II values (about 1/100 solar). The resulting (U-B) color excess allows such objects to be easily identified in large field samples. But stars with abundances significantly lower than 1/100 solar are not distinguishable in broad band measures because metallic line absorption is so small. Search techniques for these are based instead on narrow band photometry of the Ca II "K" band, for instance.

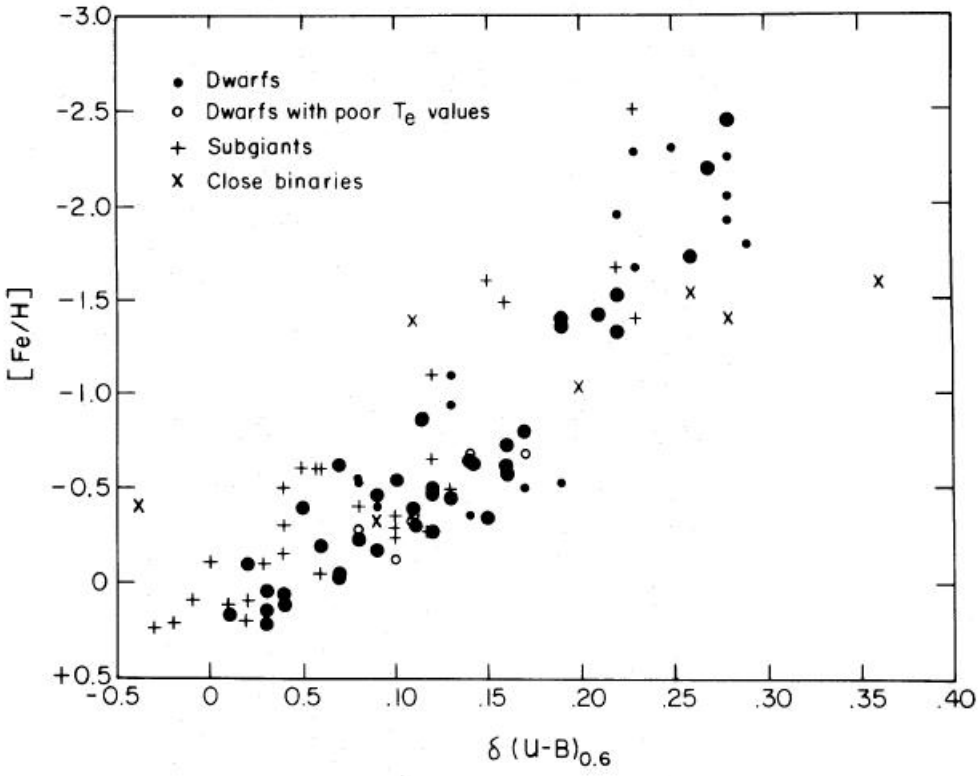

UV Excess vs. Metallicity (Carney 1979)

II. COLORS OF COMPOSITE STELLAR POPULATIONS

The composite, integrated light of unresolved stellar systems, such as galaxies and distant star clusters, is usually analyzed with the help of "spectral synthesis" models, which combine the light of individual stellar types in the appropriate mixtures.

The composite spectral energy distribution (SED) is given by

$$F(\lambda) = \sum n_j s_j(\lambda)$$

where s_j is the SED for stars of type j and n_j is the number of such stars in the population. The luminosity zero point is often unimportant, so it is usually best to normalize the SED's to a standard wavelength such as the V band. In flux-ratio form, this expression becomes:

$$G(\lambda) = \sum p_j f_j(\lambda)$$

where p_j is the fractional contribution of type j to the total light at V, $G = F(\lambda)/F(V)$, $f = s_j(\lambda)/s_j(V)$, and $\sum p_j = 1.0$.

Such computations are usually done for high to moderate spectral resolution ($\sim$ 1-30 Å), based on "libraries" of observed spectra for nearby stars or of theoretical synthetic spectra from model atmospheres.

Broad-band colors can be obtained for composites either by integrating the filter responses over a high spectral resolution sythetic model or by directly combining the flux ratios corresponding to the colors of the component stars (e.g. $f(B) = 10.0^{-0.4(B-V)}$).

One property of such composites in the standard 2-color UBV diagram is that they will always lie above and to the right of the locus for individual stars.

There are many grids of synthetic spectra for composite populations available on the web, with varying degrees of sophistication and fidelity. A series of SED's for a single-burst population with a 1 Gyr duration viewed at different ages is shown in a later figure. The SED for any possible star formation history can be synthesized by a combination from a sufficiently fine-grained grid of single-generation models.

COMPOSITE POPS (continued)

The goal of spectral synthesis analysis is to extract information on the chemical abundance structure and star formation history (SFH) of distant stellar populations. Abundances and SFH must be simultaneously determined, since they are strongly linked. Wavelength "leverage" is very important in this process. A long wavelength baseline allows you to "dissect" the population, since stars of different types dominate different wavelengths.

A subsequent plot illustrates "dissection" for an old (> 5 Gyr) population.

In the V-band ($\sim$ 5500 Å) the red giant branch and main sequence turnoff make comparable contributions. Derived population parameters (age, abundances) depend on good modeling of evolutionary rates and surface gravity effects.

In the mid-UV ($\sim$ 2200-3200 Å), the turnoff stars dominate. This is the most sensitive region to age.

In the near-IR ($>$ 8000 Å), the red giant branch and aysymptotic giant branch stars (K and M types) dominate (not shown). In general, these are more sensitive to abundance than age.

Except in hotter populations, there are almost no "pure" absorption features, and feature blending must be properly modeled. Blending is, in general, less serious at longer wavelengths.

In the far-UV ($<$ 2000 Å), the minority populations of low mass stars on the hot and "extreme" horizontal branch dominate in old populations. These are sensitive to age and metal abundance and also to helium abundance.

Note that lower main sequence ($\lesssim 0.7 M_\odot$) stars are <u>never</u> very important at any wavelength. Yet the LMS usually contains most of the <u>mass</u> of the population. Determining the mass of a population from its SED therefore requires extrapolation of the stellar mass function and is highly model-dependent. The ratio of mass-to-light (M/L) is least subject to evolutionary effects in the K-band (2.2μ).

In younger populations ($<$ 1 Gyr):

Massive main sequence stars become more important at all wavelengths. The Balmer lines and Jump are among the best age indicators.

M supergiants are very important in the near-IR for a small range of ages $\sim$10-25 Myr. They are a strong marker for this age range.

In very young populations ($\lesssim$ 8 Myr), containing stars $\gtrsim$ 5 $M_\odot$ capable of strong ionization, emission lines become important. These can be used to estimate the total far-UY ionizing luminosity and hence the star formation rate.

Younger populations are, unfortunately, often involved in dust, so correction for extinction effects (as well as emission line contamination) is important to determining stellar properties.

SED changes for a single generation are roughly proportional to the logarithm of age. It is most appropriate to think of analyzing the SFH of a population in terms of bins which are equally spaced in log(t).

The subsequent pages show applications of synthesis models to the problem of both young, star-forming galaxies and old, quiescent galaxies.

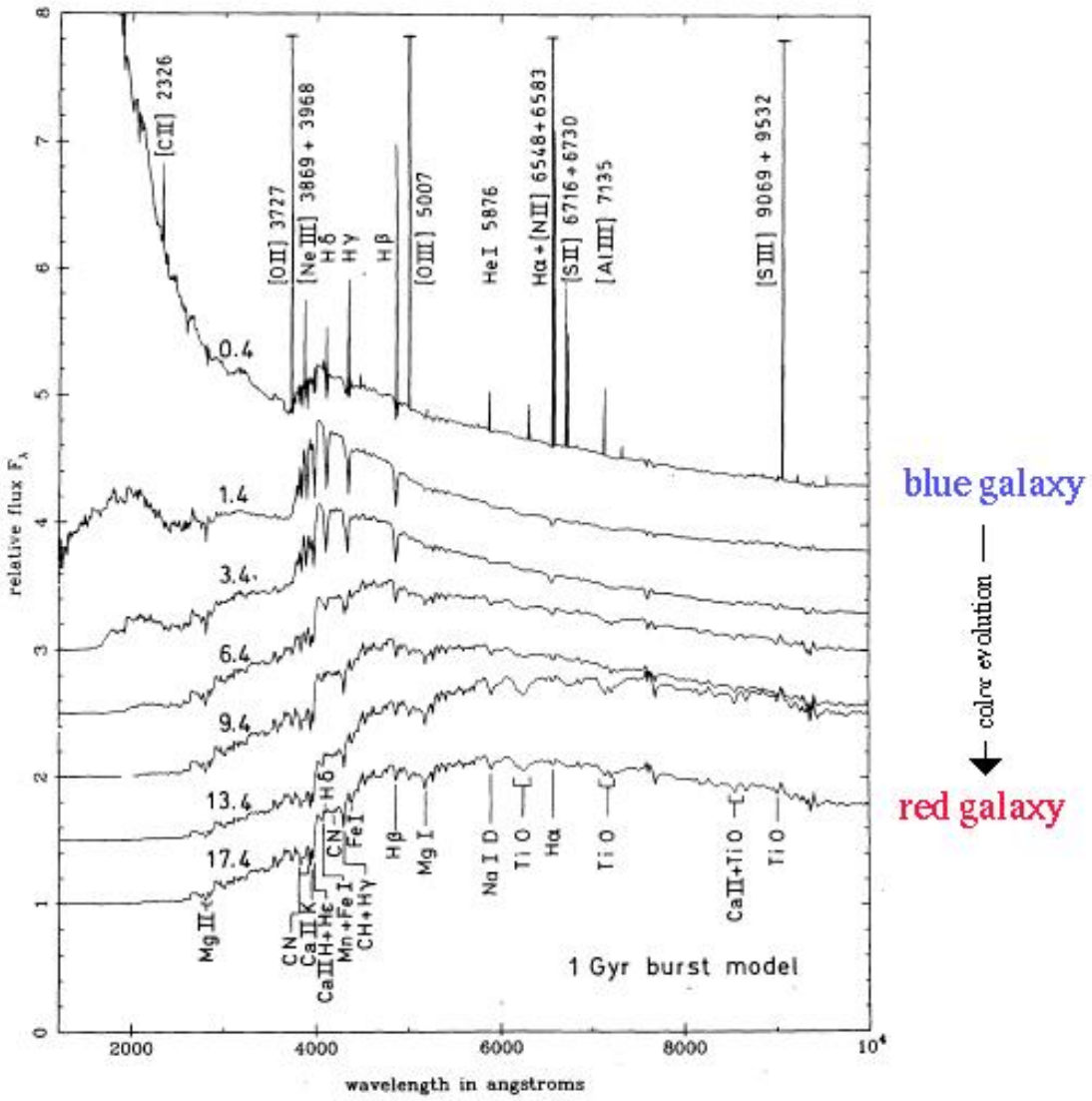

Synthetic spectra predicted for a burst population (1 Gyr duration) viewed at different ages (listed in Gyr at the left hand side).

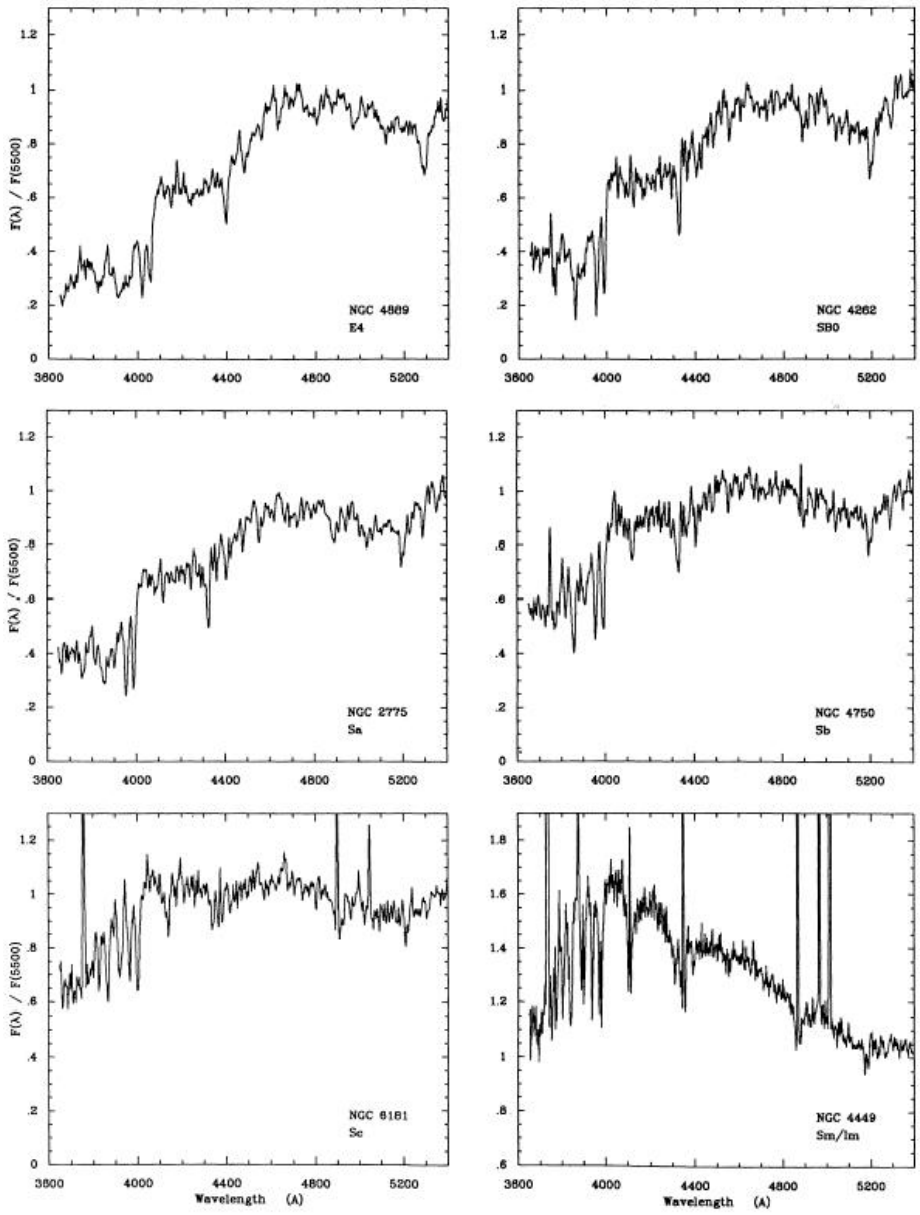

Integrated spectra of selected bright galaxies (Kennicutt 92)

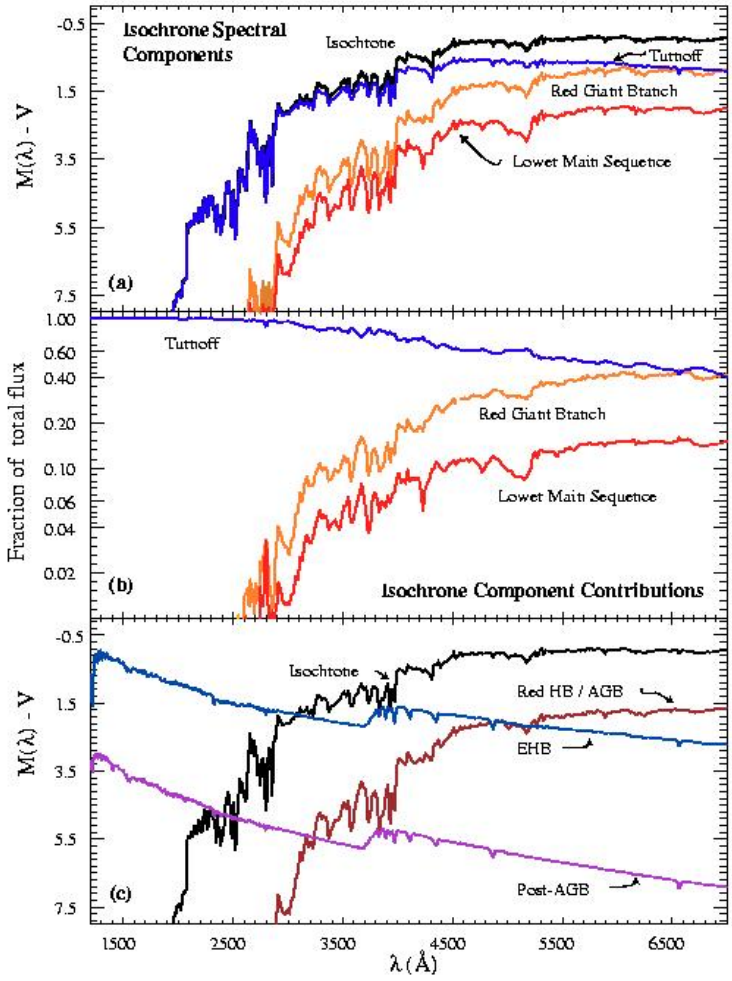

Wavelength "Dissection" of Population Components in the Integrated Light of Old Population

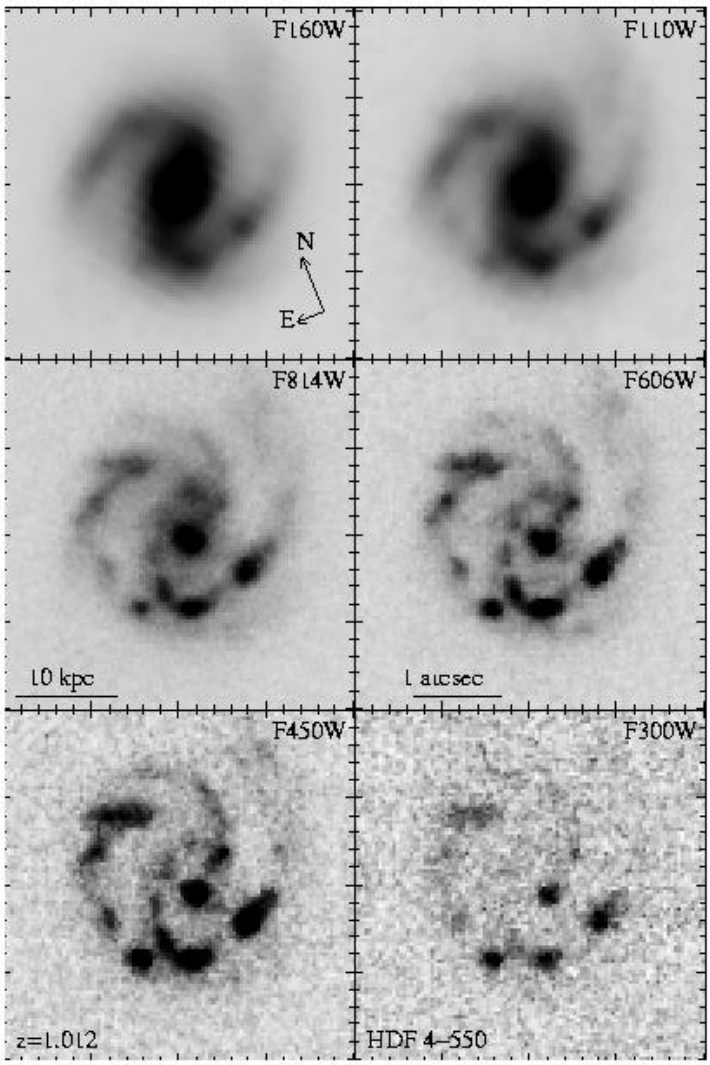

Multiband Population Dissection in Image of Redshift ∼1 Galaxy (Bunker 1999)

HST images from the Hubble Deep Field. Lab-frame filter wavelengths listed: in four lower panels in nm units; in two upper panels, in 10 nm units. Rest-frame wavelengths are half the lab-frame values.

Dramatic morphological changes occur from the rest-frame near-IR (top) to the UV (bottom).

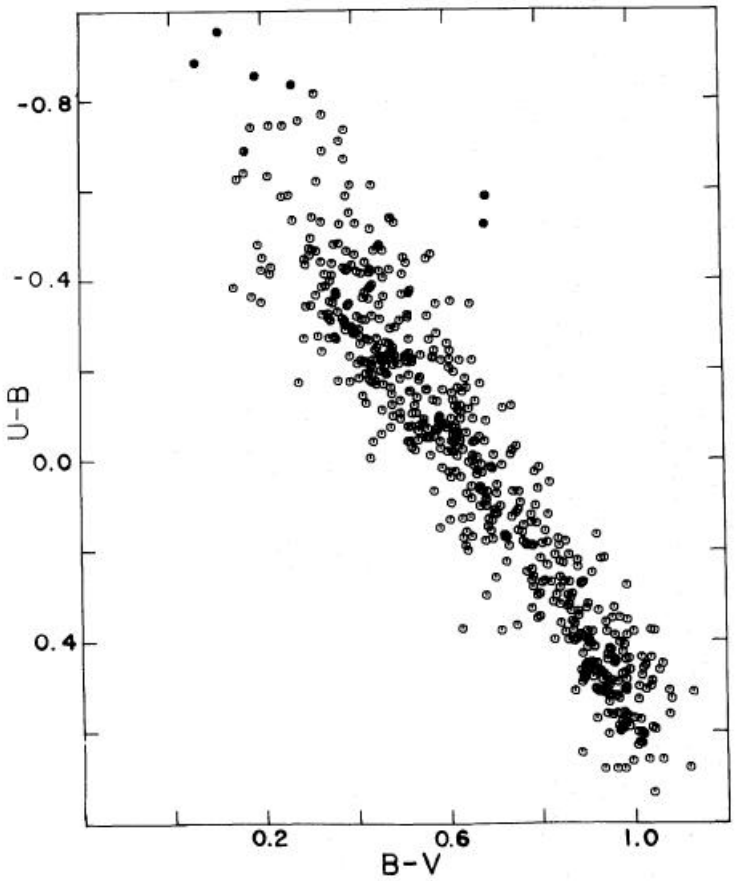

FIG. 1.—The two-color distribution of galaxies. The data include measurements of field galaxies from de Vaucouleurs (1961) and de Vaucouleurs and de Vaucouleurs (1972), Markarian galaxies from Huchra (1977*a*), Zwicky galaxies from Sargent (1970), and Haro galaxies from Du Puy (1968, 1970). The filled circles near the top of the diagram represent observations of parts of galaxies—H II regions—by Huchra (1977*a*, *b*) and Sandage and Tammann (1974*b*).

Observed colors of blue galaxies, dominated by younger populations, in the two-color diagram (Huchra 1977)

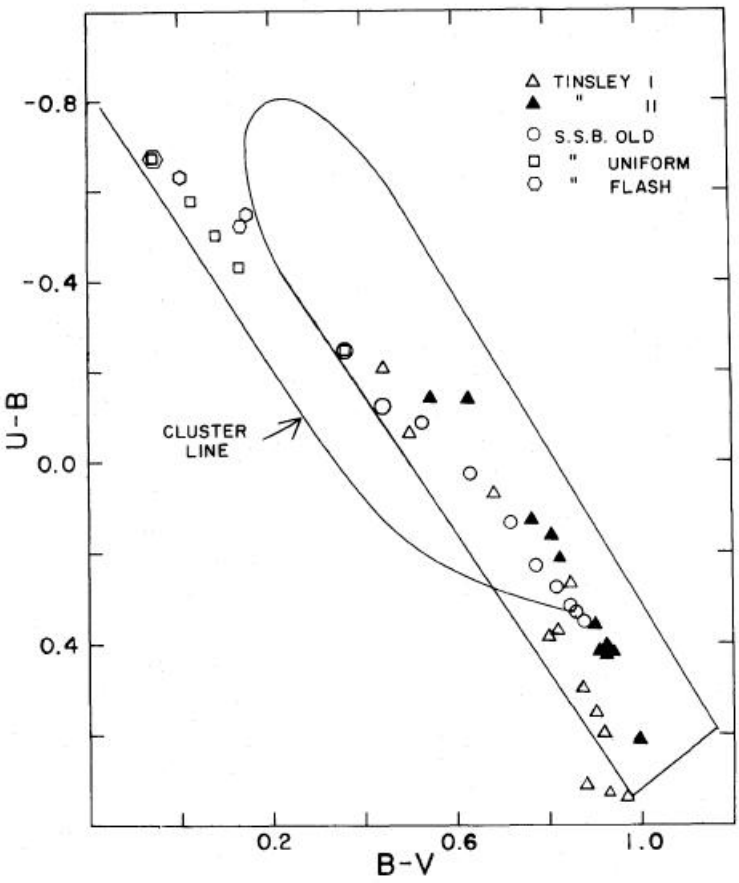

FIG. 2.—Colors for existing models of galaxies superposed on the observed envelope of galaxy colors from Fig. 1. The open and filled triangles are for models from Tinsley (1968, 1972); open circles, squares, and hexagons are from old, uniform, and "flashing" galaxy models by Searle *et al.* (1973). Also shown is the evolutionary track for star clusters with an initial delta function star-formation rate (Searle *et al.* 1973).

Synthetic models for young pops in the two-color diagram (Huchra 1977).

The outline shows the empirical color envelope from the preceding plot. The models do not overlap the blue tip of the envelope. Only models involving strong, short-lived bursts of star formation in old populations fit there. This was among the first evidence that the star formation history of galaxies can be strongly discontinuous.

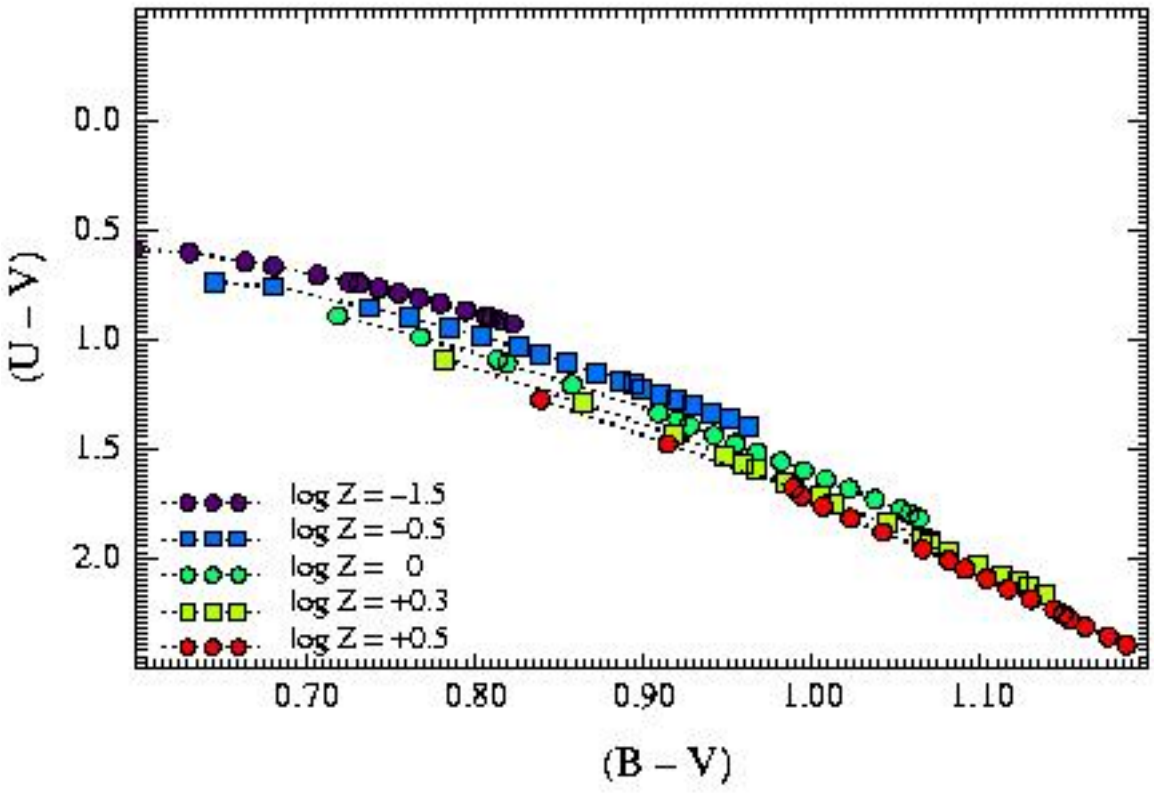

Old population colors in standard UBV (DOR 03), showing a small degree of age/abundance separation

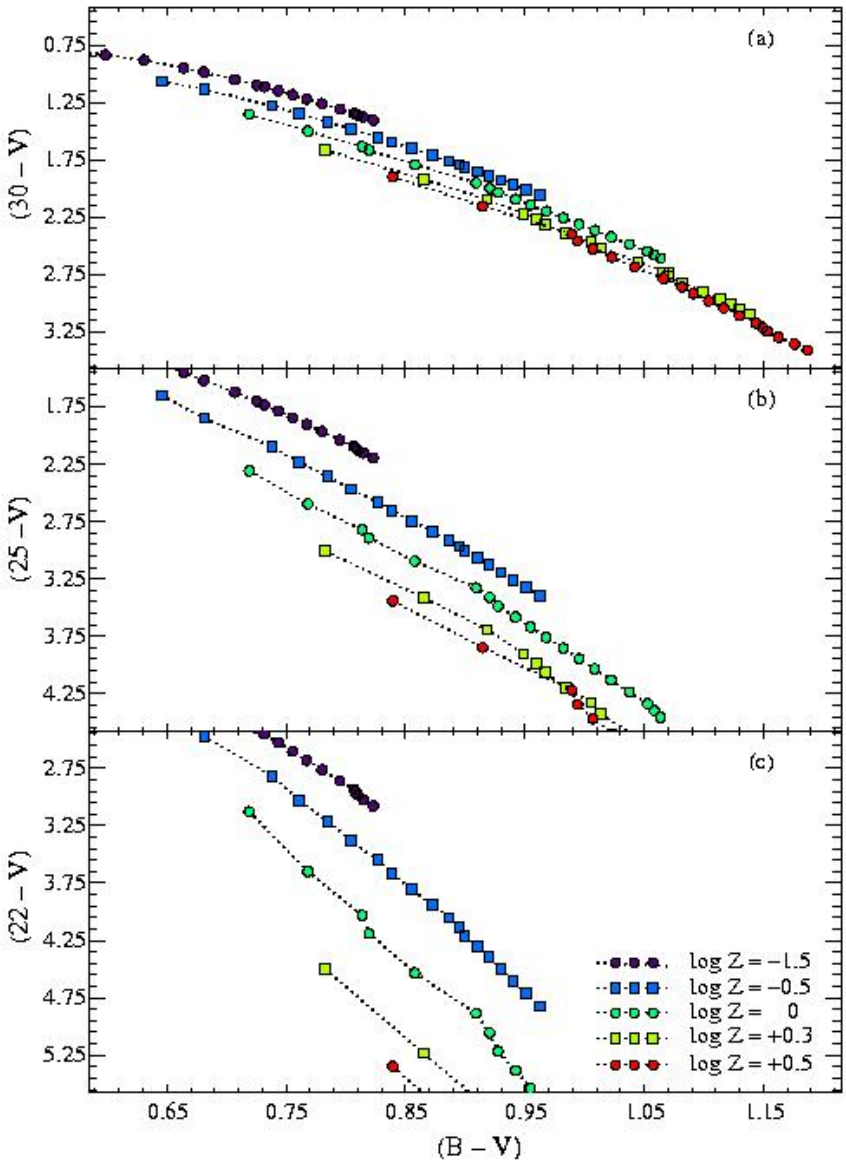

Old population colors in the Mid-UV (DOR 03), showing much better age/abundance separation

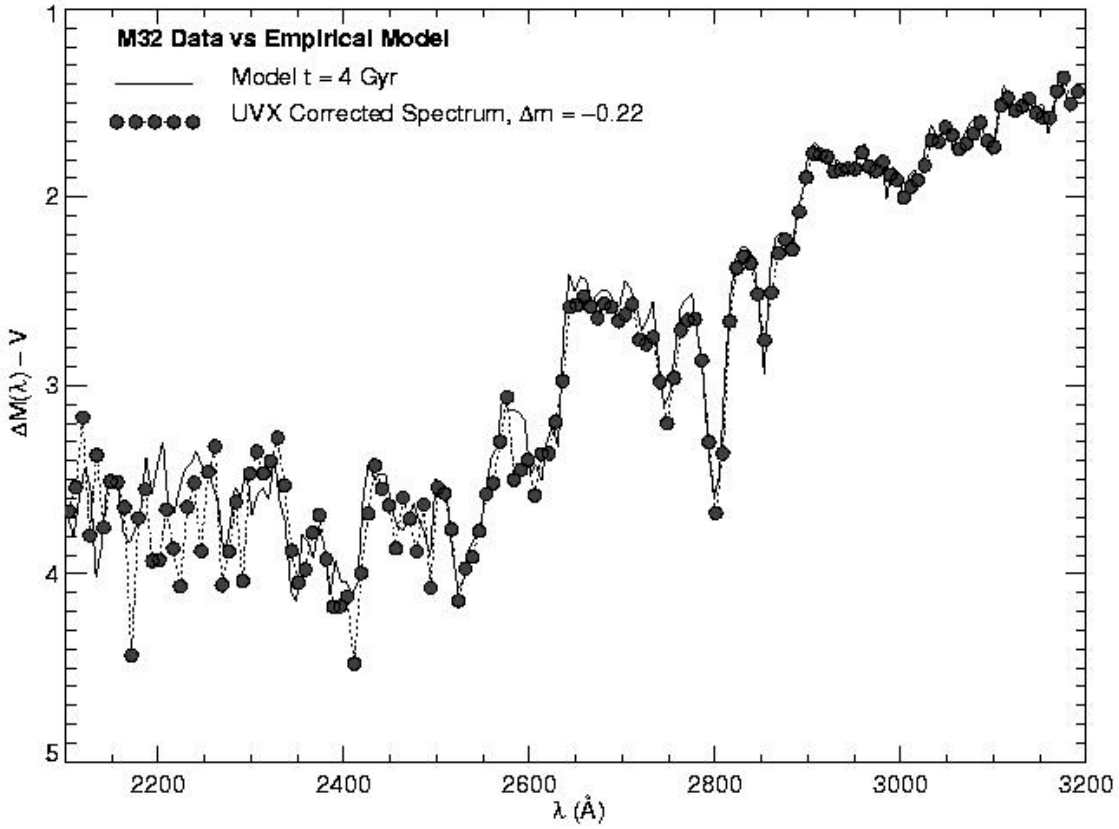

Fit of 4 Gyr old, solar abundance synthetic model to the mid-UV spectrum of elliptical galaxy M32 (DOR 03).

This is evidence (now widespread) for "intermediate-age" star formation in early type galaxies, possibly induced by mergers or tidal captures involving gas-rich neighbors.

III. INTERSTELLAR EXTINCTION

Interstellar extinction is caused by dust grains. Typical grain properties were described in Lecture 4. Grain opacities are generally higher at shorter wavelengths, so the net effect of extinction is to "redden" spectral energy distributions by removing excess blue light.

The optical depth of grains in a given direction can be written $\tau(\lambda) = n_g \, L \, \kappa(\lambda)$

...where n_g is the number density of grains per unit volume in the ISM, κ is the effective radiative cross-section per grain (cgs units cm^2), and L is the pathlength

According to the equation of transfer for a "foreground screen" of dust in front of a source with intrinsic intensity I_o (and assuming no significant thermal radiation or scattering from grains at the wavelengths involved), the emergent specific intensity is decreased as follows: $I = I_o \, e^{-\tau(\lambda)}$, or converting to magnitudes:

$$m(\lambda) = m_o(\lambda) + 1.086 \, n_g \, L \, \kappa(\lambda)$$

Typical extinction in the V-band is about 1 mag per 2×10^{21} gas atoms cm^{-2} in our Galaxy.

The wavelength dependence of the grain opacity is called the "extinction law" or "reddening curve"

Detailed dependence of the law has been determined by photoelectric filter photometry or spectrophotometry of pairs of stars with same spectral types but different colors [e.g. Whitford 1958].

It is traditional to normalize the extinction law to its difference between the B and V band wavelengths, as follows. (Notation here is non-standard.)

$$\zeta(\lambda) \equiv \frac{\kappa(\lambda)}{\kappa(B) - \kappa(V)}$$

and then rewrite the magnitude increase from extinction as:

$$A(\lambda) \equiv m(\lambda) - m_o(\lambda) = E(B-V) \, \zeta(\lambda)$$

where $E(B-V)$ is known as the "(B-V) color excess" and characterizes the amount of extinction toward a given source.

EXTINCTION (continued)

ζ will be the same for all sources as long as the character of the dust grains is the same.

$\zeta(V)$ is also known as "R", the "ratio of total to selective extinction."

For the kind of dust prevalent in the diffuse interstellar medium of our Galaxy, $R \sim 3.1$ and

$$\zeta(\lambda) \sim -0.98 + \frac{2.24}{\lambda_\mu}$$

where λ_μ is the wavelength in microns. This relation is a fair approximation for the range 4000–10250 Å. Outside of this region, the extinction law shows significant curvature.

The dust extinction law has been found to vary from place to place in our Galaxy and to differ between galaxies. It is especially subject to variations at ultraviolet wavelengths and in young star-forming regions.

For a complete description of ζ see Savage & Mathis (ARAA, 17, 73, 1979) and Cardelli, Clayton & Mathis (ApJ, 345, 245, 1989). The latter paper gives careful fitting formulae which can be used to estimate the extinction law for any R. The IDL Astronomy Users Library program `ccm_unred` is the easiest way to access the CCM formulae.

Reddening effect on sources in the UBV two-color diagram:

Reddening effects on broad bands are usually estimated as though all the light is emitted at the mean wavelength of the bands.

The slope of the reddening trajectory in UBV is

$$\frac{\Delta\,(U-B)}{\Delta\,(B-V)} = 0.72$$

Since OB stars often suffer significant extinction, this creates a diffuse envelope of sources running downward from the intrinsic hot star locus. Reddening trajectories are straight lines in this diagram.

As long as the reddening and temperature vectors are at a significant angle to one another, one can obtain a unique solution for a hot star's color by backtracking along the reddening vector. Note that the method gives ambiguous results for redder objects.

EXTINCTION (continued)

Other geometries:

Since 1980 it has become apparent that the preceding simple description of extinction by a foreground screen does not adequately capture the behavior of complex sources, such as star-forming regions observed in external galaxies. This is often encountered in UV observations, since the grain opacity is highest there.

Different dust/star geometries and photon scattering must be considered, and these can produce very different effects than the foreground screen case.

For example, if the dust and stars are uniformly mixed together (e.g. in a compact, young star cluster), then referring to Lecture 4 we find that:

$$I(\lambda) = I_o(\lambda)\,\frac{1 - e^{-\tau(\lambda)}}{\tau(\lambda)}$$

Here, I_o is the intensity from the source that would be observed in the absence of internal dust and τ is the total optical depth in dust.

In this situation we see light from approximately one optical depth into the source, and the visible volume will increase with wavelength because the opacity decreases with wavelength.

The reddening trajectory for this geometry is very different than for the foreground screen. For a discussion of such effects and their influence on observations, see the Calzetti (2001) review and Witt, Thronson, & Capuano (1992).

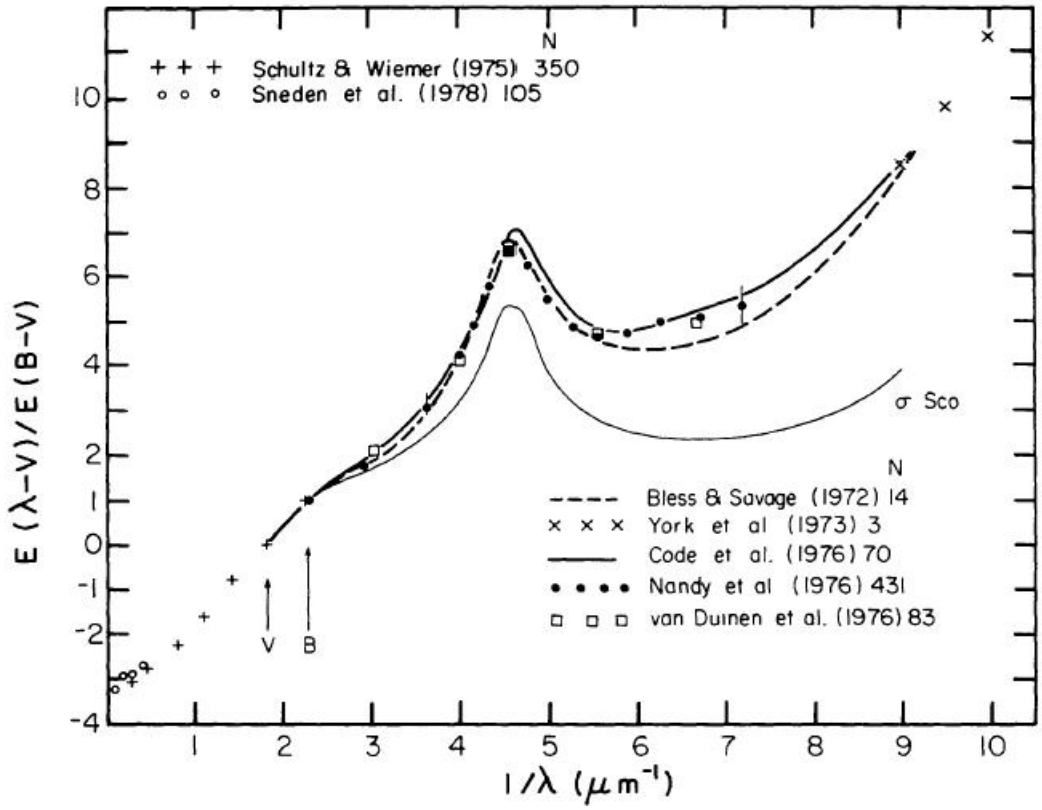

Mean Extinction Law (Savage & Mathis 1979)

Note the large range in extinction over the IR-to-UV bands. The UV "2175 Å bump" is characteristic of extinction laws in our Galaxy and the LMC. But it is absent along some sightlines and in the SMC and is frequently absent in other galaxies. It probably originates in small, carbonaceous grains which are sensitive to the surrounding environment.

Table 2 An average interstellar extinction curve

	$\lambda(\mu m)$	$\lambda^{-1}(\mu m^{-1})$	$E(\lambda-V)/E(B-V)$	$A_\lambda/E(B-V)$
	∞	0	−3.10	0.00
L	3.4	0.29	−2.94	0.16
K	2.2	0.45	−2.72	0.38
J	1.25	0.80	−2.23	0.87
I	0.90	1.11	−1.60	1.50
R	0.70	1.43	−0.78	2.32
V	0.55	1.82	0	3.10
B	0.44	2.27	1.00	4.10
	0.40	2.50	1.30	4.40
	0.344	2.91	1.80	4.90
	0.274	3.65	3.10	6.20
	0.250	4.00	4.19	7.29
	0.240	4.17	4.90	8.00
	0.230	4.35	5.77	8.87
	0.219	4.57	6.57	9.67
	0.210	4.76	6.23	9.33
	0.200	5.00	5.52	8.62
	0.190	5.26	4.90	8.00
	0.180	5.56	4.65	7.75
	0.170	5.88	4.77	7.87
	0.160	6.25	5.02	8.12
	0.149	6.71	5.05	8.15
	0.139	7.18	5.39	8.49
	0.125	8.00	6.55	9.65
	0.118	8.50	7.45	10.55
	0.111	9.00	8.45	11.55
	0.105	9.50	9.80	12.90
	0.100	10.00	11.30	14.40

Tabulated Mean Extinction Law (Savage & Mathis 1979)

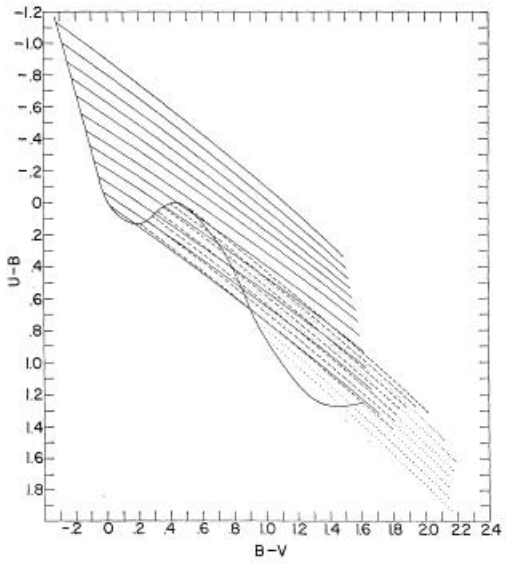

FIG. 4. Reddening trajectories in the color–color diagram terminated on the intrinsic relationship for luminosity class V stars.

Reddening Trajectories in Two-Color Diagram (Wildey 1963)

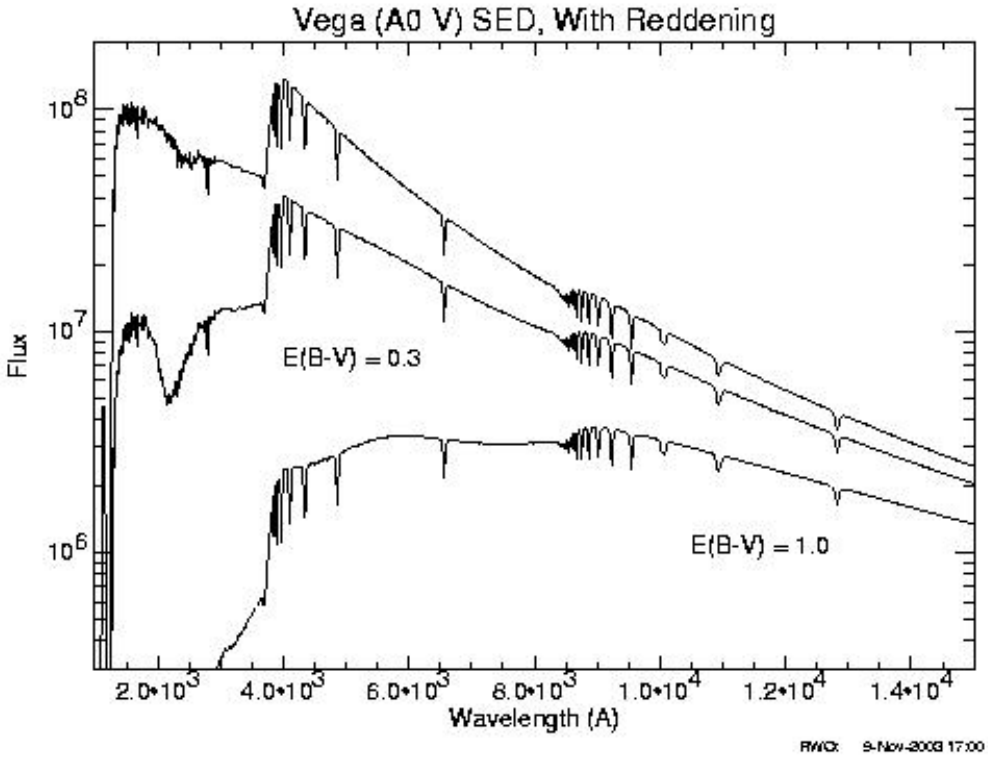

Reddening Effects on SED of Vega

Extinction sufficient to produce a (B-V) color excess of 1.0 mag has a drastic distorting effect on the SED of sources at wavelengths below 1 micron.

For cases of large optical depths and broad bands, especially where the intrinsic SED in not smooth, the effect of extinction changes appreciably within the band. Here, it is important to actually integrate the extincted SED in order to estimate net reddening effects.

IV. REDDENING-INDEPENDENT INDICES

Because the shape of the extinction law (outside the UV region) does not change much in the diffuse interstellar medium, it is possible to define reddening-independent color combinations for the foreground screen case. These "Q" indices will be the same for an unreddened source as for a heavily extincted one. You need to measure magnitudes in at least three bands to define Q indices.

A typical Q index is defined as follows:

$$Q \equiv (m_1 - m_2) - q_{123}\,(m_2 - m_3)$$

where $q_{123} = \left[\frac{\zeta_1 - \zeta_2}{\zeta_2 - \zeta_3}\right]$

You can verify that this index does not change with the total extinction to the source.

Q parameters are useful, for example, in studying star clusters in other galaxies which may suffer large amounts of extinction.

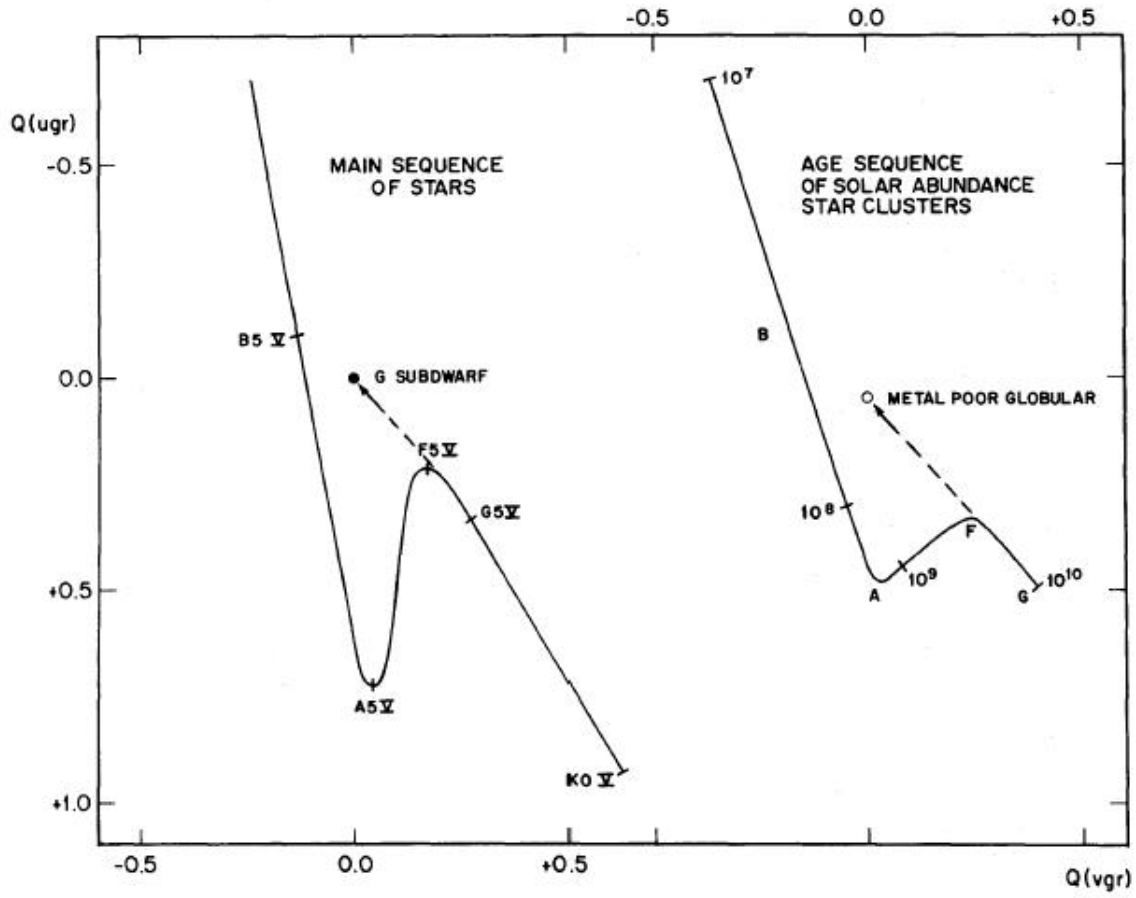

Searle-Wilkinson-Bagnuolo (1980) QQ Population Diagram

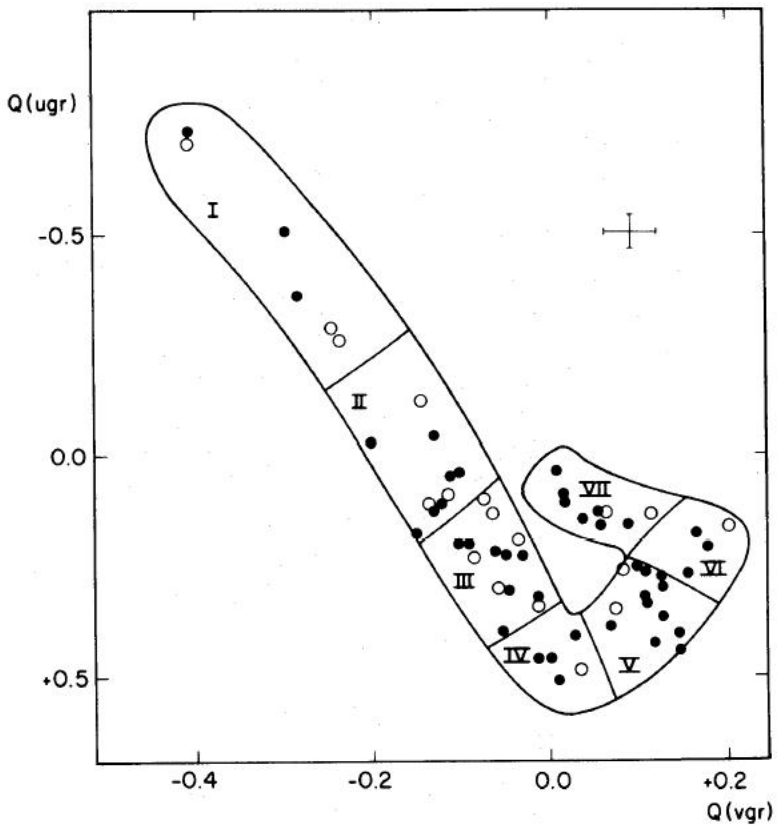

FIG. 3.—Populous clusters of the Magellanic Clouds in the Q-Q plane. Open and closed circles represent clusters of the SMC and LMC, respectively. The Cloud clusters form a sequence in this diagram. The sequence has been arbitrarily segmented, and the zones drawn in this figure define a classification scheme.

Magellanic Cloud Intrinsic Cluster Population Categories (SWB 80)

V. EXAMPLE: SUPER STAR CLUSTER AGES/EXTINCTIONS

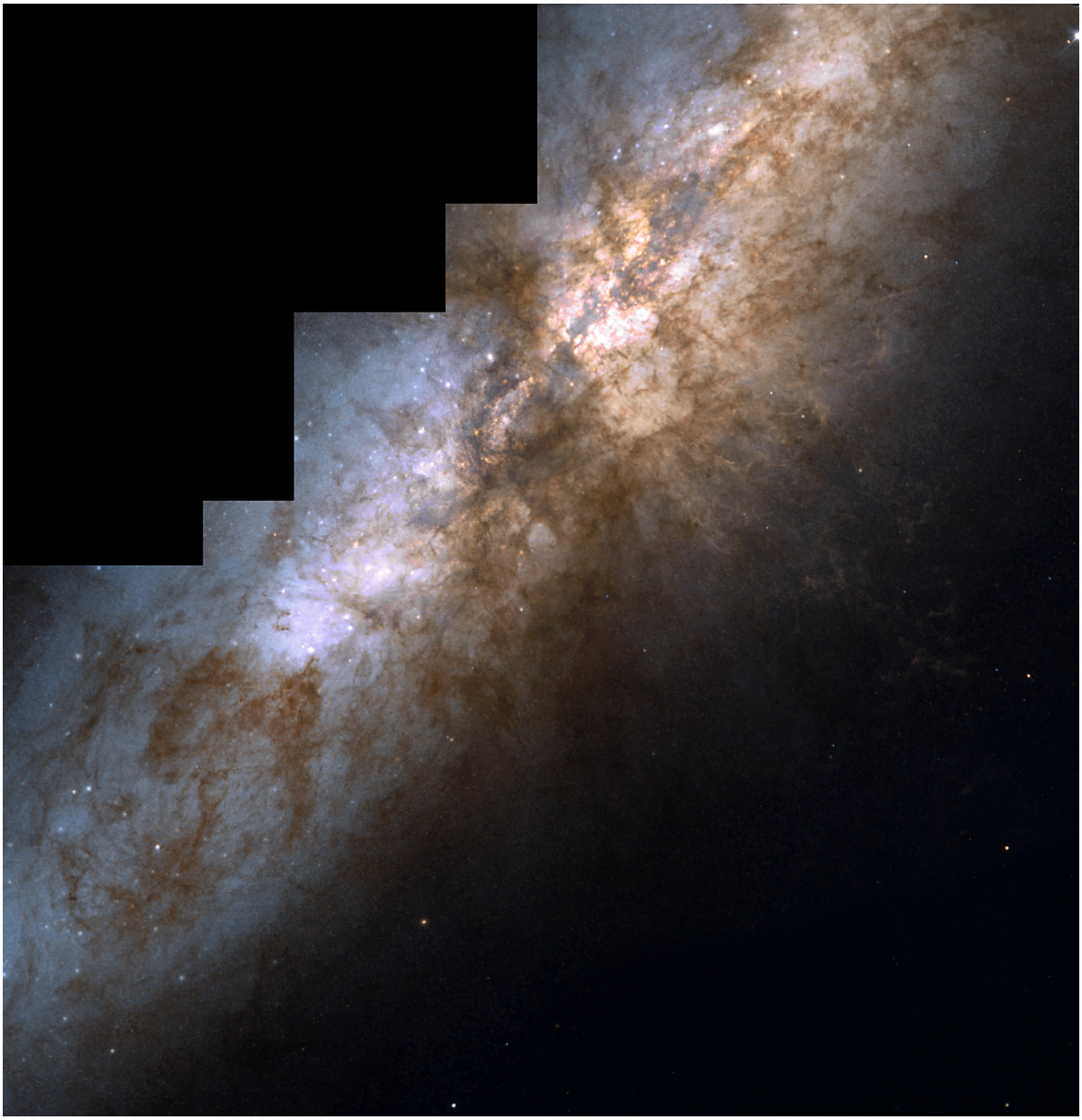

Color Composite Image of M82

Shows resolution of the starburst galaxy M82 into luminous, young star clusters with HST/WFPC2. Pinkish clumpy structures to upper right of central dark lane are the near side of the starburst region, which is mostly heavily obscured ($A_V \gtrsim 5$).

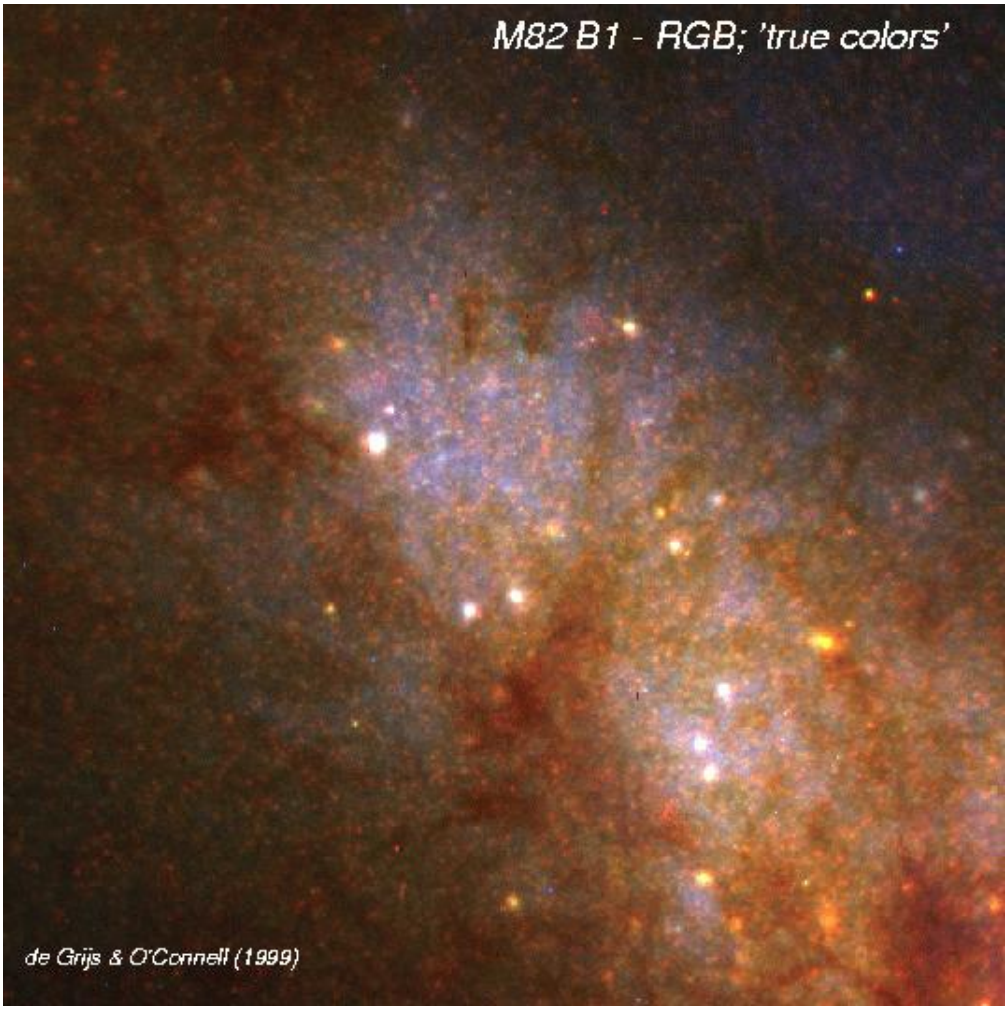

M82 Region B1 Showing Resolved Super Star Clusters

Closeup of the lower left wing of the preceding image. This region is about 1 kpc from the current starburst activity and is the site of a "fossil" starburst.

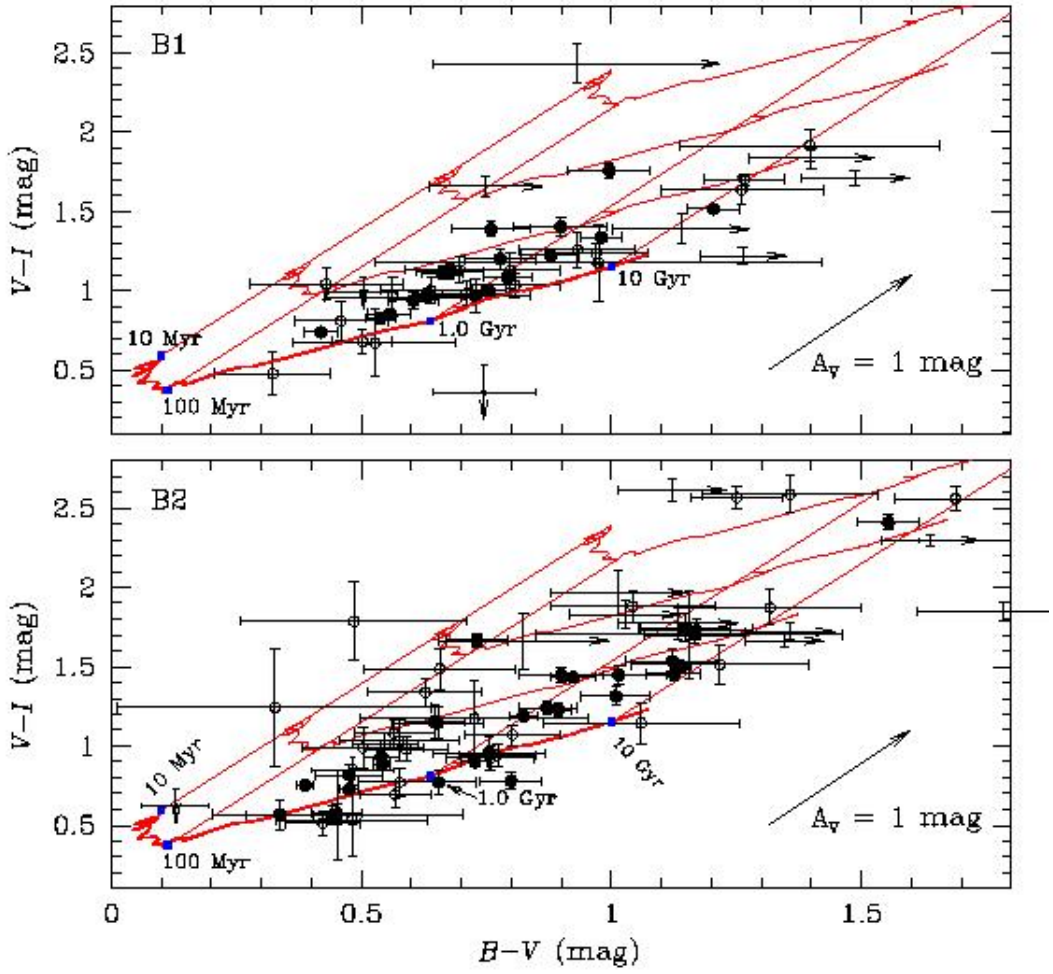

Two-Color Diagram of Clusters in M82 B1 and B2

This diagram, based on multiband images of the B1 and B2 regions, plots the BVI colors of each cluster detected. Because the "ageing" and "extinction" vectors are not parallel, it is possible to simultaneously solve for age and extinction for each cluster. There is considerable differential extinction across B1 and B2, so a common foreground dust screen model is inapplicable.

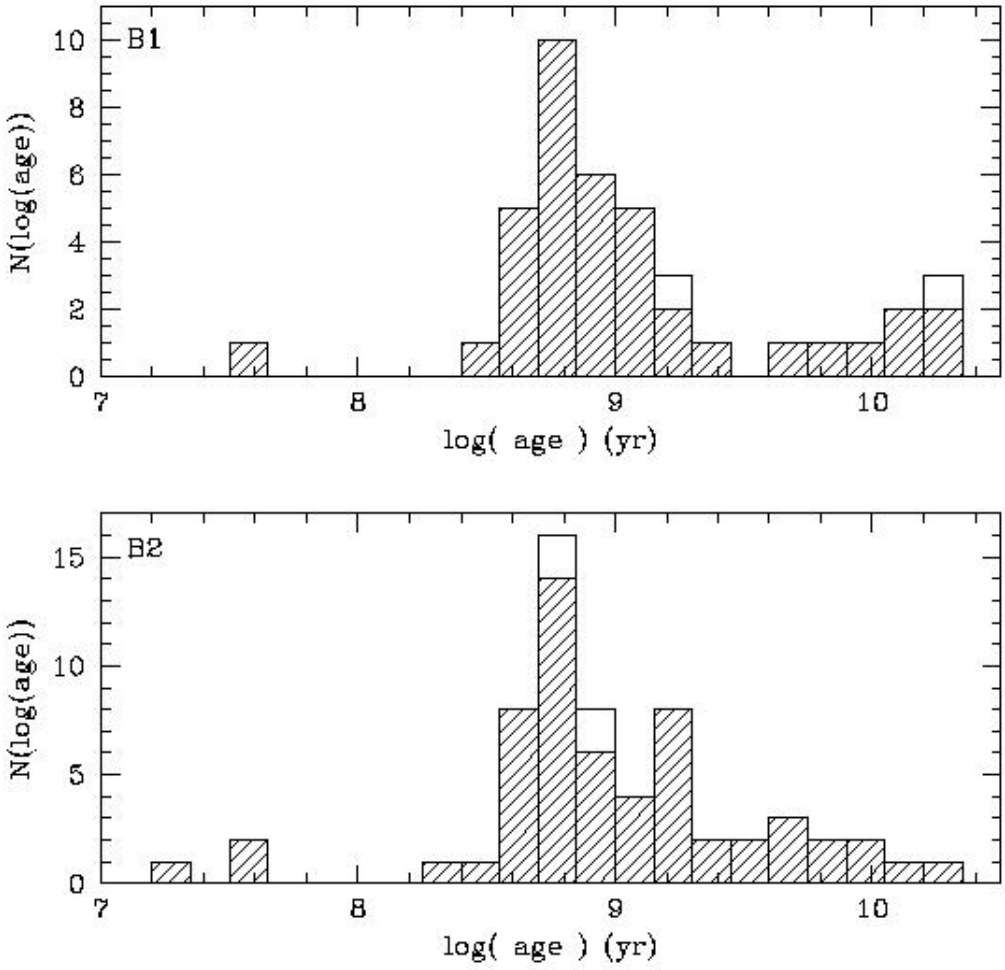

M82 Fossil Starburst: Derived Age Histogram

Histogram shows a burst of cluster formation at $\sim$ 600 Myr ago, which happens to coincide with a tidal passage of companion galaxy M81. Little SF has occurred since in this region, whereas there is a massive ongoing starburst in the galaxy's center (age $\lesssim$ 50 Myr).

VI. EXAMPLE: PHOTOMETRIC REDSHIFTS

One can use the distinctive features in broad-band spectral energy distributions of distant galaxies to obtain approximate values of their redshifts from their multi-band colors alone.

The main useful features are (1) the spectral slopes as a function of rest wavelength; and (2) the large discontinuities at rest wavelengths near 4000 Å (known the "H&K break" or the "4000 Å break"), which occurs in populations of almost all ages, and near 910 Å (the "Lyman break"), which is visible only in younger populations. There is also a sharp decline in the SED of distant younger populations below Lyα at 1216 Å caused by the intervening "forest" of hydrogen clouds.

The redshifts so determined are called photometric redshifts (or "photo-z's"). A large amount of effort has gone into modeling galaxy SEDs and testing the precision possible with photometric redshifts. With good data this is estimated to be $\sigma(z) \lesssim 0.03$.

The technique requires a simultaneous fit to the intrinsic spectral shape (determined by the stellar population and dust) and to the shift in wavelength space.

A major application is to star-forming systems at high redshift (z $\gtrsim$ 3) which are detectable by their Lyman continuum and Lyα breaks. Broad-band images of such objects become dark (or "drop out") at wavelengths below the break. [This technique obviously selects against objects with large UV extinctions.]

Another is to search for high redshift analogs of low-redshift quiescent galaxies (e.g. giant E galaxies) as a means to determining the earliest epoch of massive galaxy formation. Again, these objects are dim in any filter that contains the restframe UV.

More precision is obtained (at a cost of longer exposure times or shallower surveys) by using intermediate-band filter sets, e.g. COMBO17, HST/WFC3.

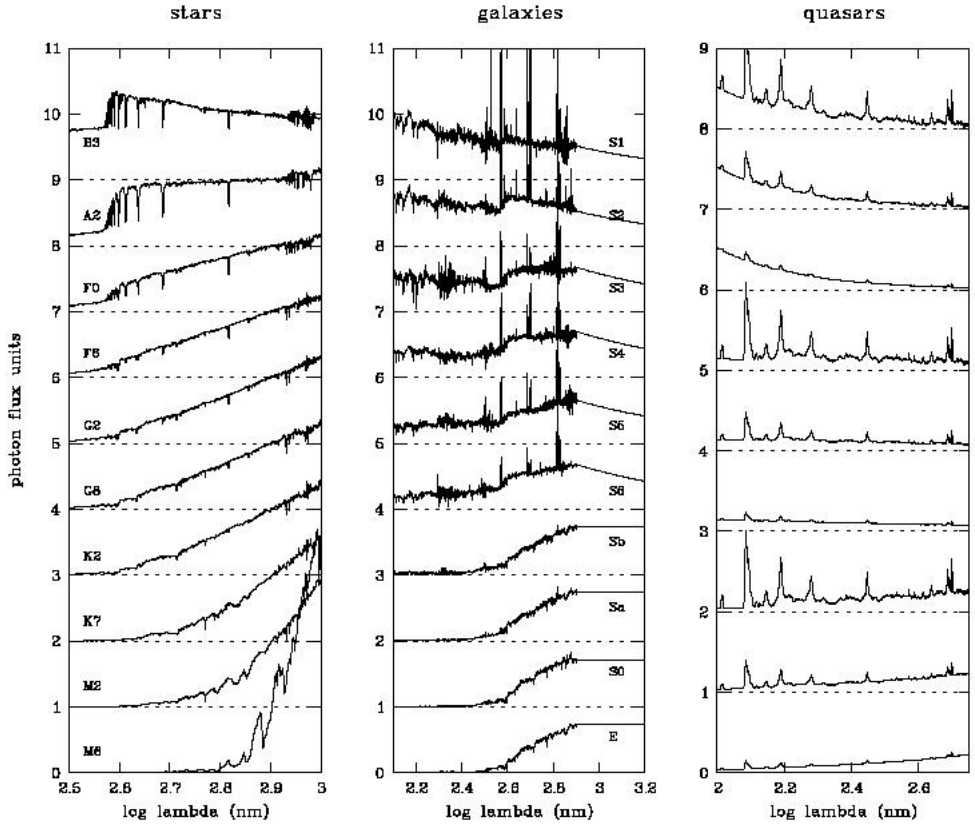

Fig. 1. This diagram shows a few selected spectra from our template libraries. The shown wavelength scale runs from 315 nm to 1000 nm for stars (left), from 125 nm to 1600 nm for galaxies (center) and from 100 nm to 550 nm for quasars (right). The flux is λf_λ in units of photons per nm, time intervall and sensitive area and offset by one unit per step within a class. The flux scale is normalised to unity at 800 nm for stars, arbitrary for galaxies, and normalised to 0.2 at 250 nm for quasars. The stellar templates are taken from Pickles (1998), the galaxy templates from Kinney et al. (1996) and quasar templates are modelled after Francis et al. (1991). The quasar diagram shows nine spectra with three different spectral indices (-2.0, -0.6, +0.8) and three different relative emission-line intensities (0.6, 2.1, 5.7).

Restframe SED's of Stars, Galaxies, QSO's

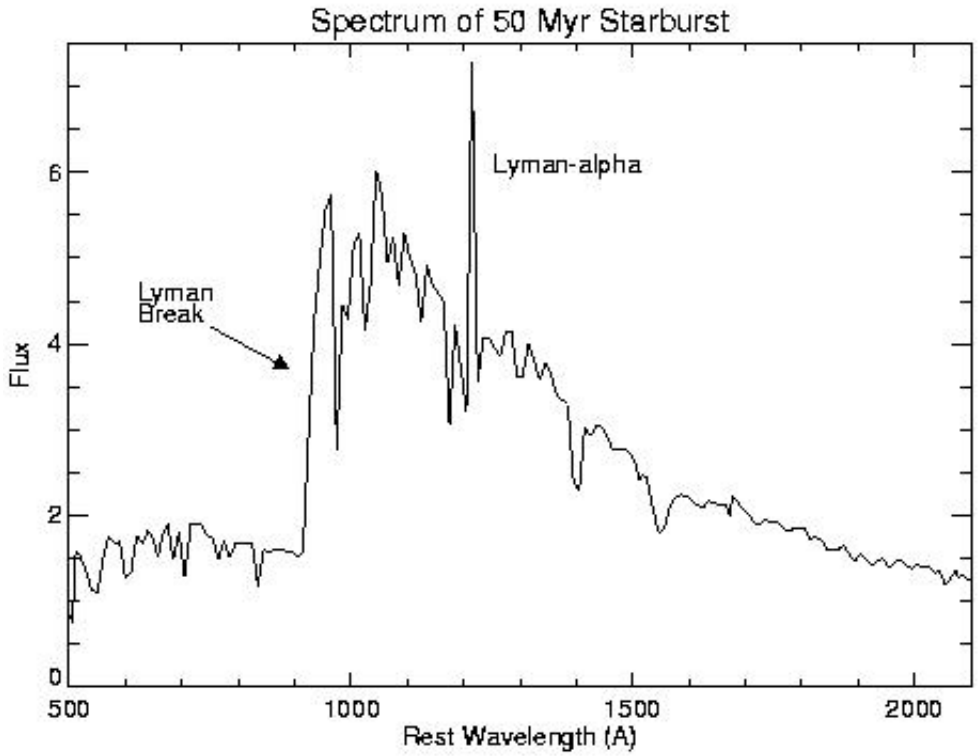

Restframe UV Energy Distribution Star Forming Galaxy

(The Lyman-α forest is not shown but would chop up the continuum shortward of 1216 Å.)

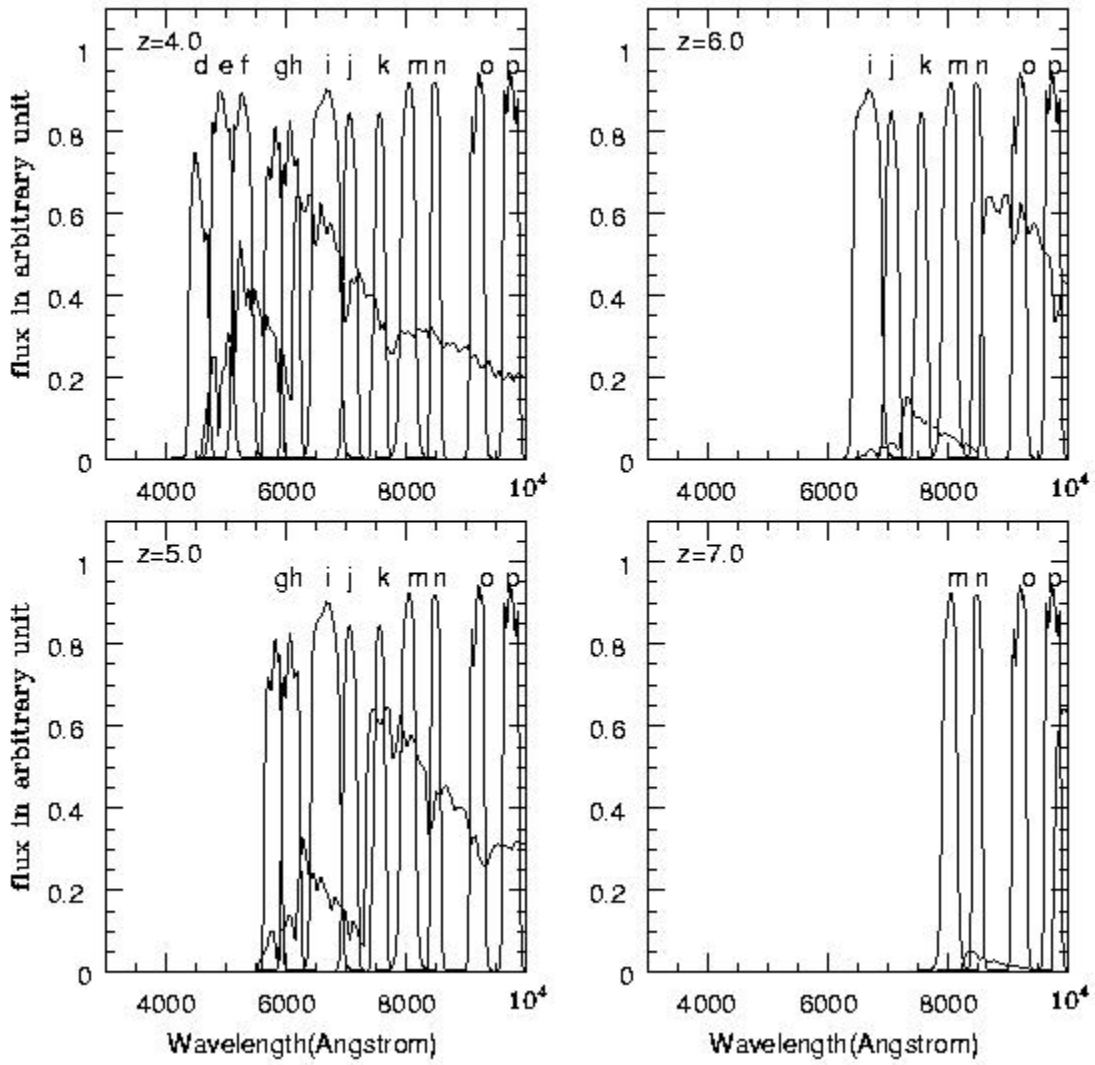

Redshifted Star Forming Galaxy SED vs Intermediate-Band Filters

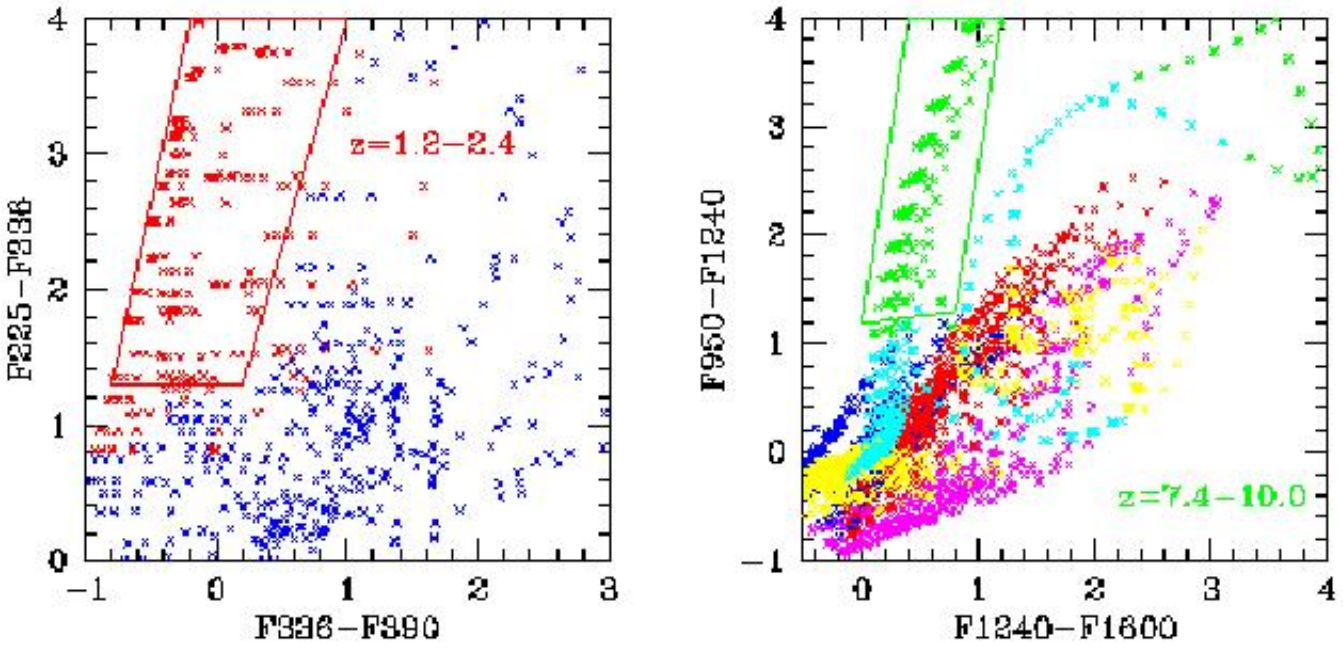

Location of High Redshift Galaxies in Two-Color Diagrams

(Based on intermediate-band filters. Color coding is for different redshift regimes)

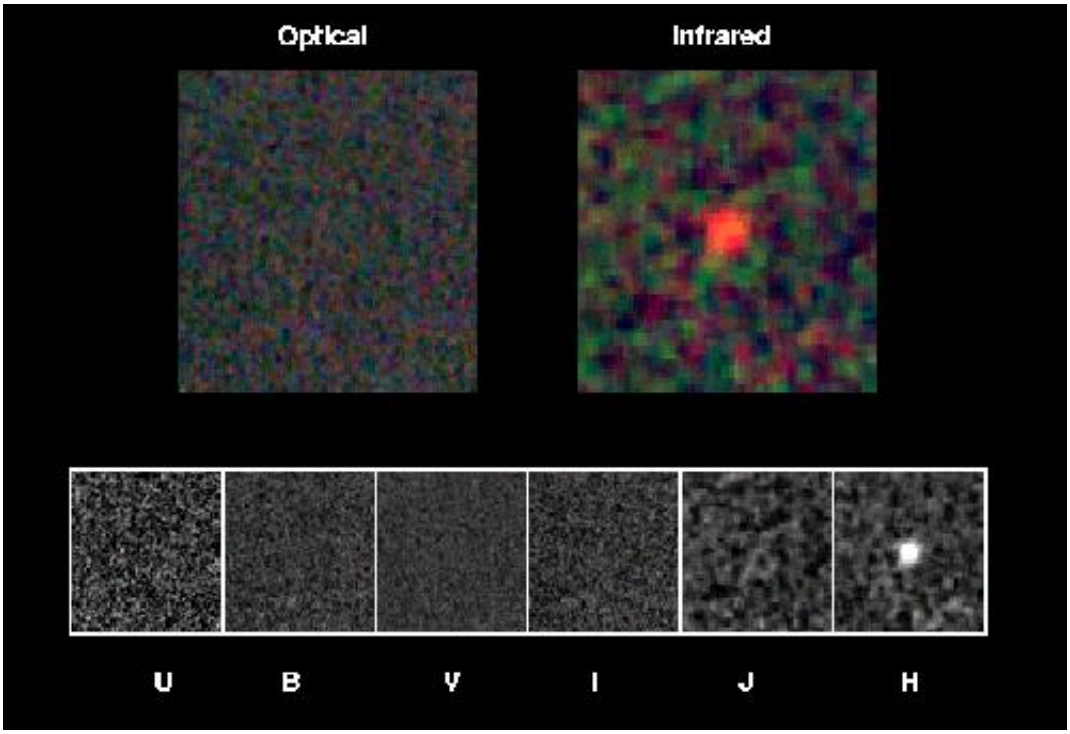

J-Band Dropout Source (Dickinson)

What redshift does this imply if the dropout is due to the Lyman break?

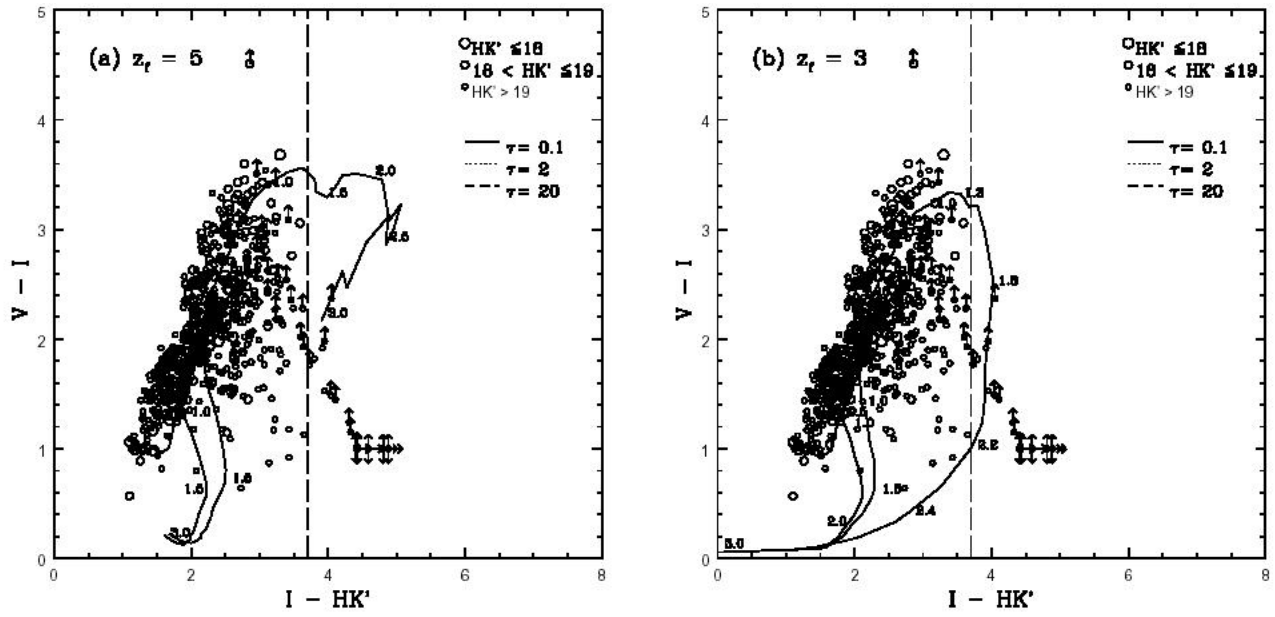

FIG. 4.—$V-I$ vs. $I-HK'$ color-color diagrams for the wide-field $HK' \leq 20.4$ sample (stars have been removed). The BC96 passively evolving model tracks folded with the appropriate V, I, and HK' filters are illustrated from $0 < z < 3$, assuming an epoch of galaxy formation of $(a)\, z_f = 5$ and $(b)\, z_f = 3$. The model tracks have been labeled with a few representative redshifts at which the various colors would be observed. The vertical dashed lines in the figures illustrate the ultrared dividing line, $I-HK' > 3.7$.

VIK search for quiescent massive galaxies at high redshift (Barger 1999)

This survey yielded few quiescent candidates (which have I-K $>$ 3.5). More recent work by McCarthy, Glazebrook, and Abraham (2004, GDDS survey) has identified such systems with more sensitive imaging and spectroscopy over large fields. Massive quiescent galaxies reside only in denser regions.

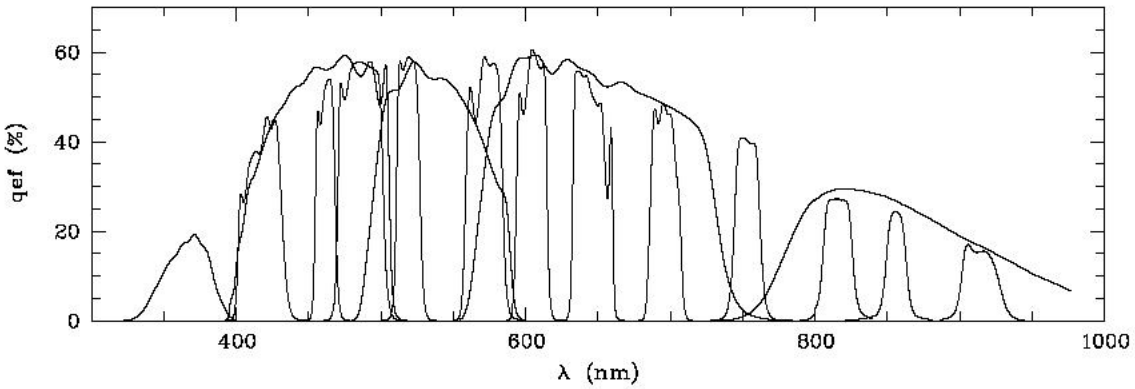

Fig. 1. COMBO-17 filter set: Total system efficiencies are shown in the COMBO-17 passbands, including two telecope mirrors, WFI instrument, CCD detector and average La Silla atmosphere. Combining all observations provides a low-resolution spectrum for all objects in the field. Photometric calibrations of such "multi"-colour datasets are best achieved with spectrophotometric standards inside the target fields.

COMBO-17 Deep Survey Interference Filter Set

VII. BROAD-BAND SKY SURVEYS

Among the most important applications of multi-band filter systems has been their use in large-scale sky surveys. Wide filters, especially when coupled to photoelectric detectors, support very deep surveys. A vast array of astrophysics has emerged from such surveys.

A. 48-in Schmidt Sky Surveys (Optical)

Prototype: Palomar Observatory Sky Survey(s)

Employ wide-field (6°) field Schmidt optics (spherical primary mirror with refractive correction lens).

Photographic: 14" plates (pressure-curved to match focal plane): pairs of exposures in 936 fields

POSS I: 1950-58. Sky north of -33°

- **103a-O: Blue (4400 Å)**
- **103a-E: Red (6500 Å) (includes Hα)**
- **Limit $\sim$ 20-21 for point sources**

Extended to southern hemisphere 1975+ by ESO/SERC

- **IIIa-J: Blue (at AAO)**
- **IIIa-F: Red (at ESO)**

POSS II: 1985 –

- **New version of Palomar-I: deeper (to $\sim$ 22 mag) and for proper motions (40-50 year baseline)**
- **IIIa-J (Blue), IIIa-F (Red), IV-N (Near Infrared)**
- **Digitized**

Digitized Sky Survey and Guide Star Survey (1985–)

- **To support HST operations, STScI digitized versions of various sets of 48-in surveys and extracted catalogues of guide stars (to $V \sim 15$). For on-line access, see:** `http://www-gsss.stsci.edu/gsc/GSChome.htm`**. Parts of these are available through the simpler SKYVIEW interface:** `http://http://skyview.gsfc.nasa.gov/cgi-bin/titlepage.pl`**.**

B. Sloan Digital Sky Survey (Optical), 2000–

Special-purpose 2.5-m telescope for imaging/spectroscopy at Apache Point, NM

Imaging of about 1/4 of sky centered on N Galactic Pole

5-color imaging using drift scanning with large CCD mosaic. Limit R $\sim$ 23. Total catalogue: $\sim$ 100 million sources

Automatic morphological discrimination of stars from galaxies using SExtractor-type software. Multicolor discrimination of QSO's from stars.

Spectroscopy (3″ diameter fibers connected to aperture plug-plate) of selected targets, including about 1 million galaxies, to R $\sim$ 18.

See `http://www.sdss.org/sdss.html`

C. Other Recent Surveys

The 2dF galaxy redshift survey conducted at the Anglo-Australian Observatory is a similar undertaking on a smaller scale in the southern sky. See: `http://www.mso.anu.edu.au/2dFGRS/`

The Galaxy Evolution Explorer (GALEX) mission (`http://www.galex.caltech.edu/`) is now performing an all-sky imaging survey to m(UV)$\sim$21 that extends these ground-based surveys to the vacuum UV.

D. 2MASS Sky Survey (Near Infrared)

Uses two 1.3-m telescopes to do deep near-IR imaging survey of entire sky.

Bands: J (1.25 μ), H (1.65 μ), K (2.17 μ).

Limiting mag: $\sim$ 15-16 (J band)

Source of accurate astrometry for detected point-like targets

Final catalogue: $\sim$ 300 million point sources, $\sim$ 1 million galaxies

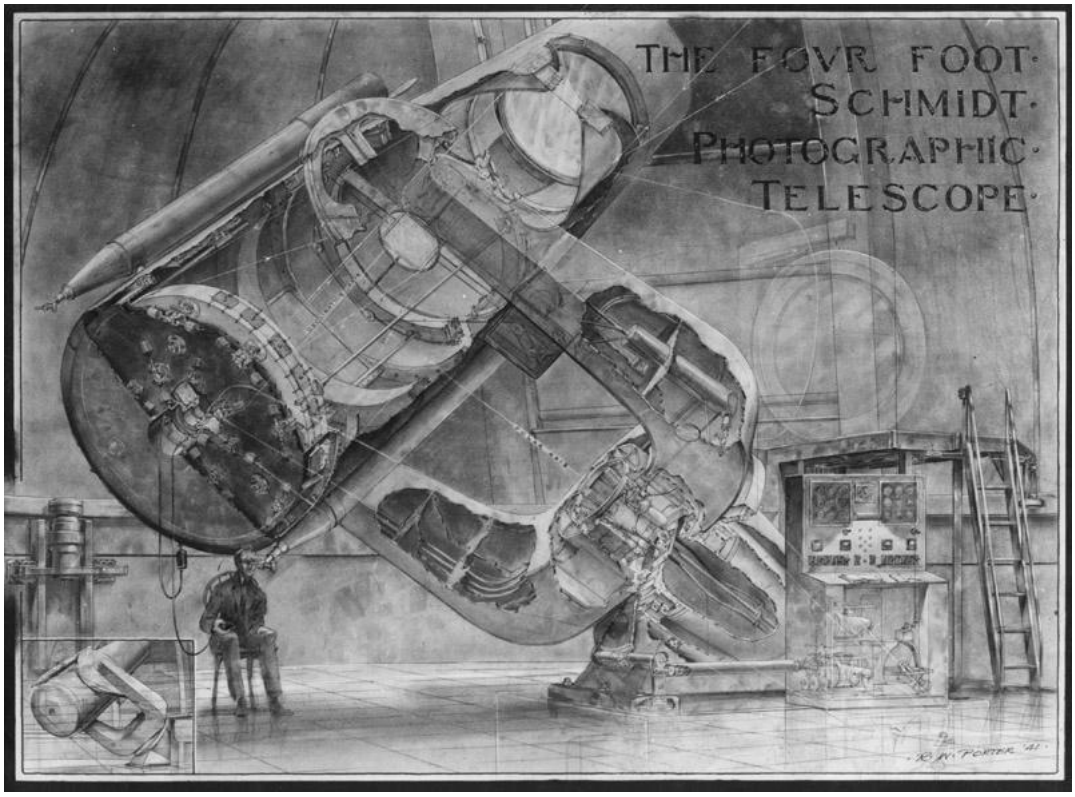

Palomar 48-in Schmidt (Porter)

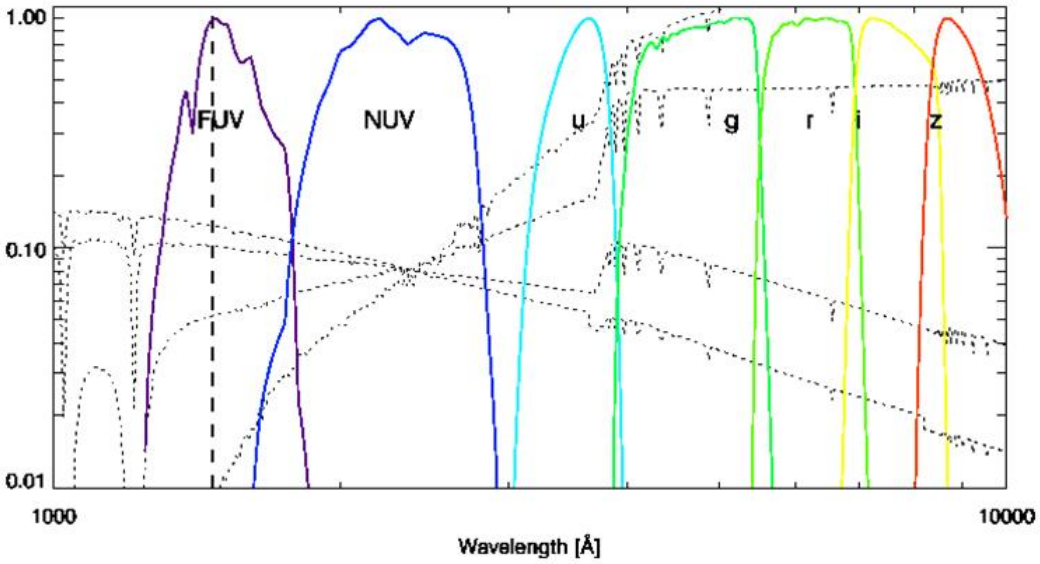

The SDSS and GALEX Filter Bands
(with sample galaxy SEDs superposed)

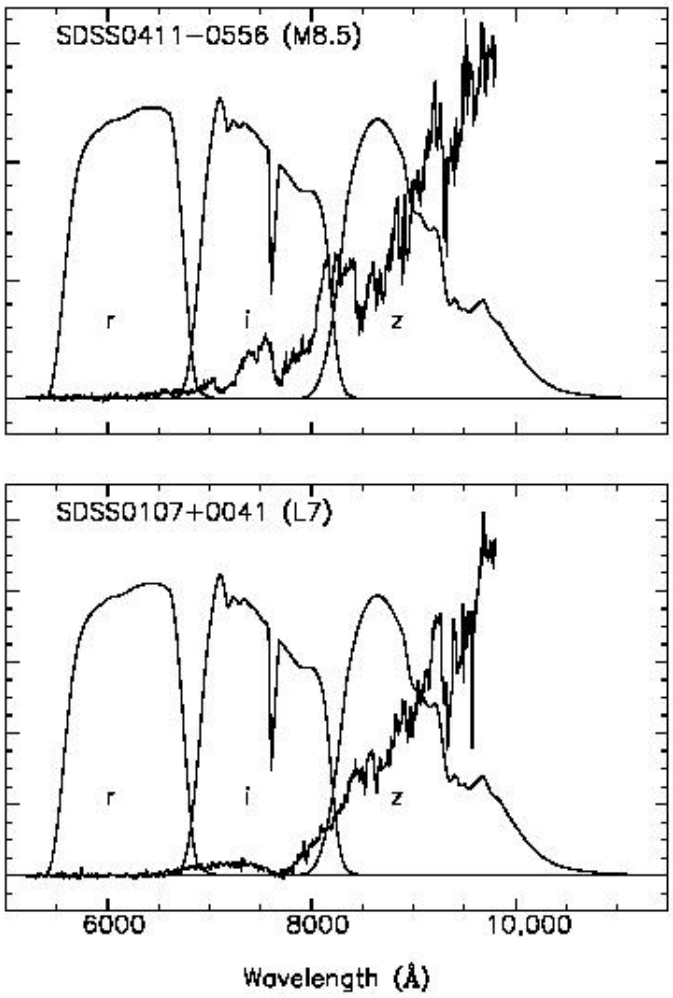

FIG. 6.—SDSS *r*, *i*, and *z* relative system responses (including 1.3 air masses) compared with HET spectra of SDSS 0411−0556 (M8.5) and SDSS 0107+0041 (L7). The strong absorption between about 8500 and 8800 Å seen in SDSS 0411−0556 is due to the 8432 and 8692 Å TiO and FeH bands, which disappear at about L3–L4 (see Fig. 4).

Cool Star SEDs in SDSS Bands

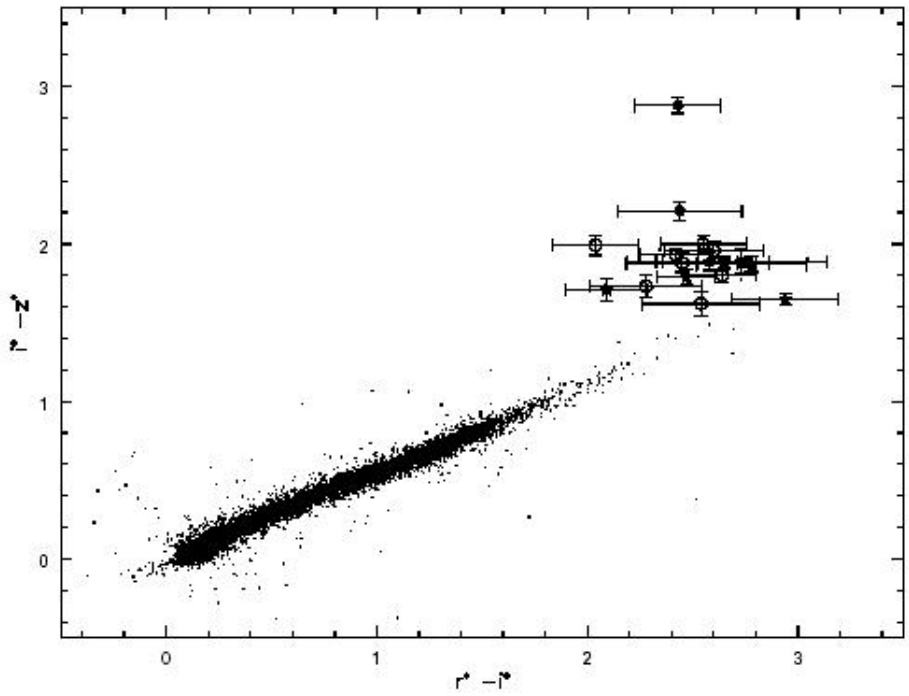

FIG. 3.—SDSS color-color plot for the 18 objects detected in all three of the *r*, *i*, and *z* bands, compared with SDSS data for 15,000 stars from Finlator et al. (2000). The symbols are the same as in Fig. 2.

Cool Star Color Separation (Brown Dwarf Candidates) in SDSS

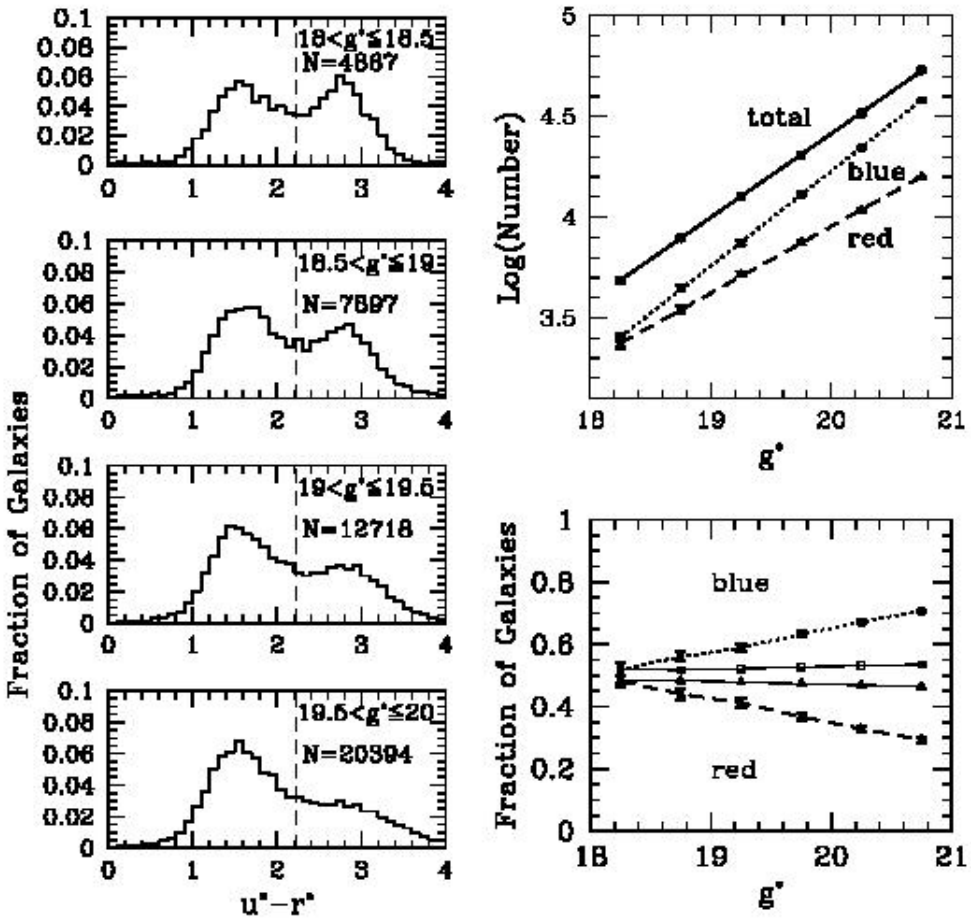

FIG. 2.—*Left*, color distribution u^*-r^* as a function of g^* magnitude of the galaxy sample; *top right*, fraction of blue galaxies (*filled squares*) increasing relative to the red (*filled triangles*) for fainter g^* samples; *bottom right*, photometric errors cannot account for the dependence of the red and blue galaxy fractions on magnitude cut. The open symbols correspond to the predicted fraction (assuming only photometric errors change with magnitude), the filled symbols to the observed.

Galaxy Color Statistics (SDSS, 2001)

Although the bimodality in colors shown here was first evident in statistics from the de Vaucouleurs *Reference Catalogs*, the SDSS provides definitive evidence for a separation between star-forming (blue) and quiescent (red) galaxies.

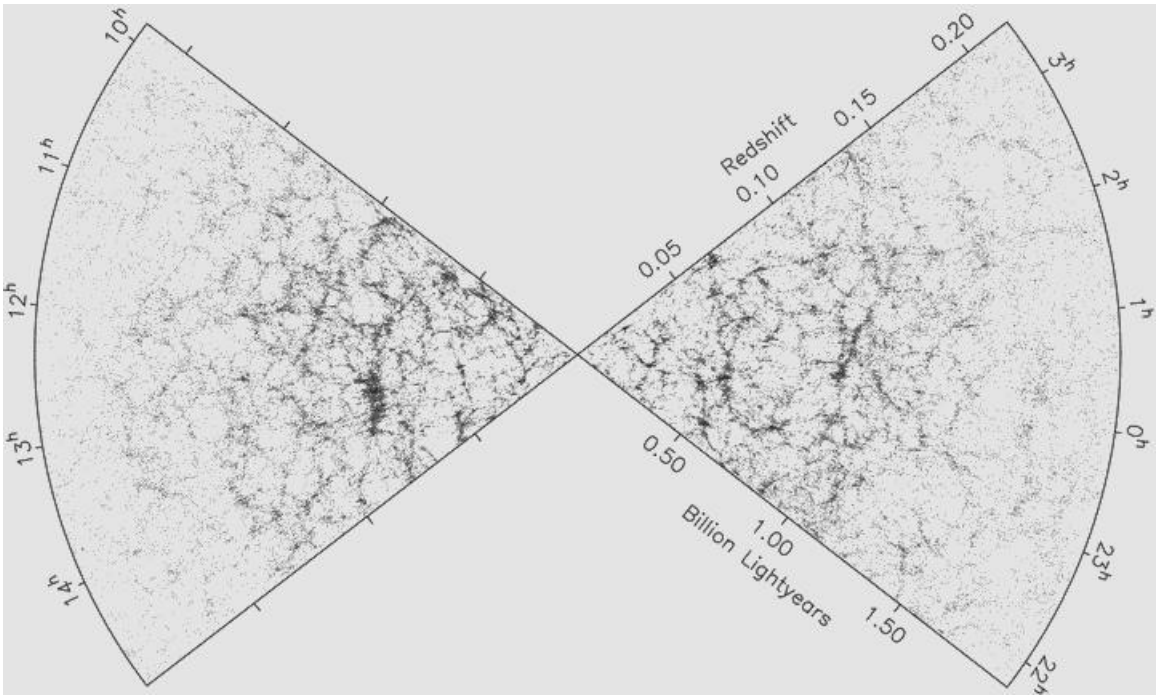

Distribution of Galaxies in the 2dF Redshift Survey (2003)

Shows the remarkable filamentary texture that only emerges in large-scale surveys.